

Comparison of tomographic wind retrievals with different geometric implementations for multistatic meteor radar networks

Supplementary Material

Loretta Pearl Poku^{1,2}, Gunter Stober^{1,2}, Witali Krochin^{1,2}, Alan Liu³, Alexander Kozlovsky⁴, Diego Janches⁵, Jie Zeng^{6,7,8}, Wen Yi^{6,7,8}, Masaki Tsutsumi^{9,10}, Njål Gulbrandsen¹¹, Satonori Nozawa¹², Mark Lester¹³, Johan Kero¹⁴, and Nicholas Mitchell^{15,16}

¹Institute of Applied Physics, University of Bern, Switzerland

²Oeschger Center for Climate Change Research, University of Bern, Switzerland

³Center for Space and Atmospheric Research, Department of Physical Sciences, Embry-Riddle Aeronautical University, Daytona Beach, Florida, USA

⁴Sodankylä Geophysical Observatory, University of Oulu, Oulu, Finland

⁵ITM Physics Laboratory, Mail Code 675, NASA Goddard Space Flight Center, Greenbelt, MD 20771, USA

⁶National Key Laboratory of Deep Space Exploration, School of Earth and Space Sciences, University of Science and Technology of China, Hefei 230026, China

⁷CAS Center for Excellence in Comparative Planetology, University of Science and Technology of China, Hefei, China

⁸Anhui Mengcheng National Geophysical Observatory and Research Station, School of Earth and Space Sciences, University of Science and Technology of China, Hefei, China

⁹National Institute of Polar Research, Tachikawa, Japan

¹⁰The Graduate University for Advanced Studies (SOKENDAI), Tokyo, Japan

¹¹Tromsø Geophysical Observatory UiT – The Arctic University of Norway, Tromsø, Norway

¹²Institute for Space-Earth Environmental Research, Nagoya University, Japan

¹³Department of Physics and Astronomy, University of Leicester, Leicester, UK

¹⁴Swedish Institute of Space Physics (IRF), Kiruna, Sweden

¹⁵British Antarctic Survey, Cambridge, UK

¹⁶Department of Physics and Astronomy, University of Leicester, Leicester, UK

Correspondence: Loretta Pearl Poku (loretta.poku@unibe.ch)

S1 Climatologies of Mean Winds Derived from SVVP Retrieval

In this section, we present a comparison of the climatological mean states of the zonal, meridional, and vertical wind components retrieved using the Velocity Volume Processing (VVP) in the plane and spherical geometries. These figures illustrate the seasonal wind climatology for all three components in both spherical (left column) and plane geometry (center column) along with their corresponding differences (right column) geometries, similar to those in figures 4 and 5, but for averaging radii of 200, 250, 300, 350, and 400 km at temporal resolutions of 15, 30, and 60 minutes.

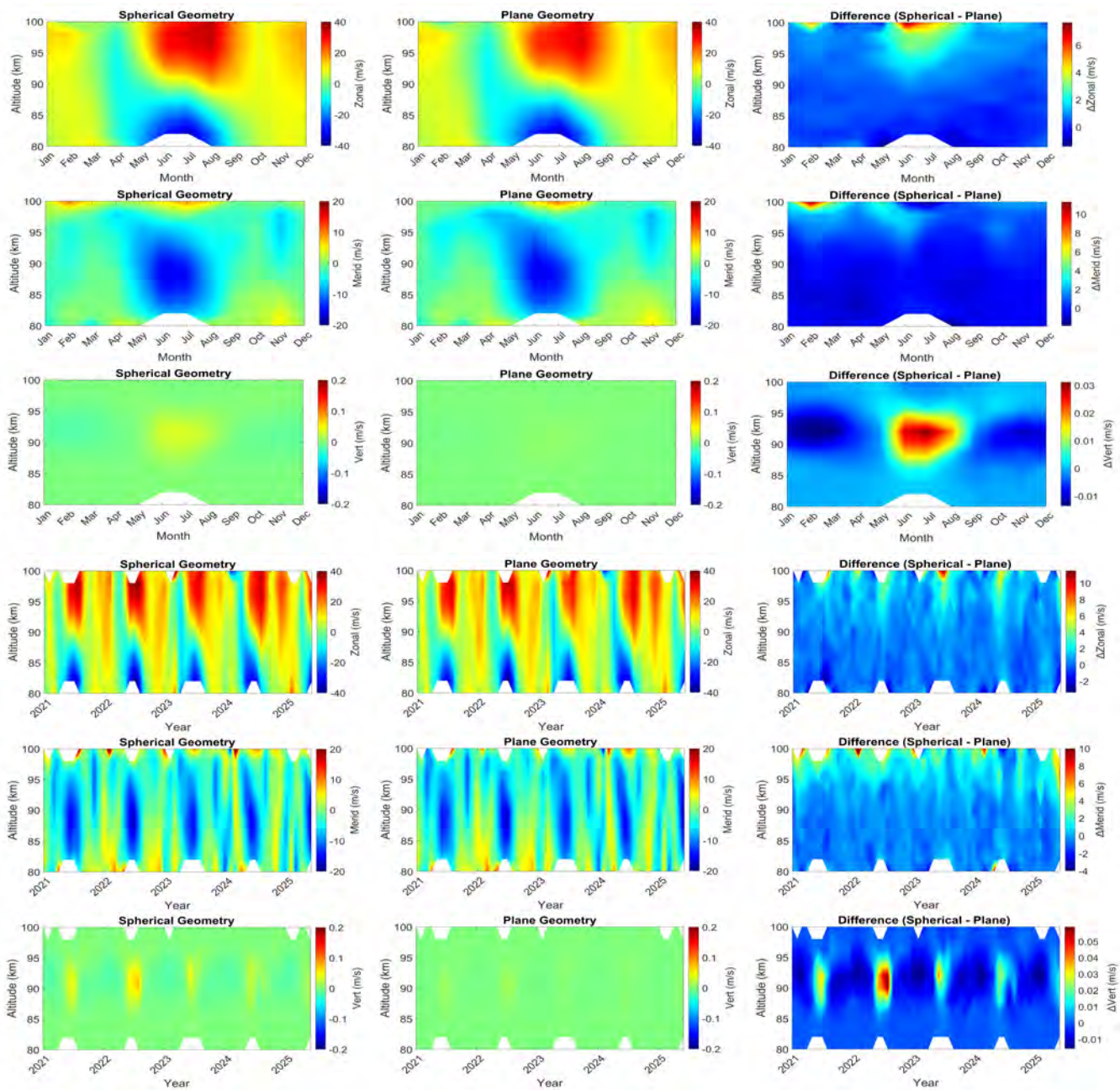


Figure S1. Composite Zonal, meridional, and vertical wind components retrieved using the Volume Velocity Processing (VVP) with 200 km averaging radius and 15-minute resolution. The first three rows show the monthly mean results; the remaining rows display seasonal averages. Each panel compares spherical geometry, plane geometry, and their differences.

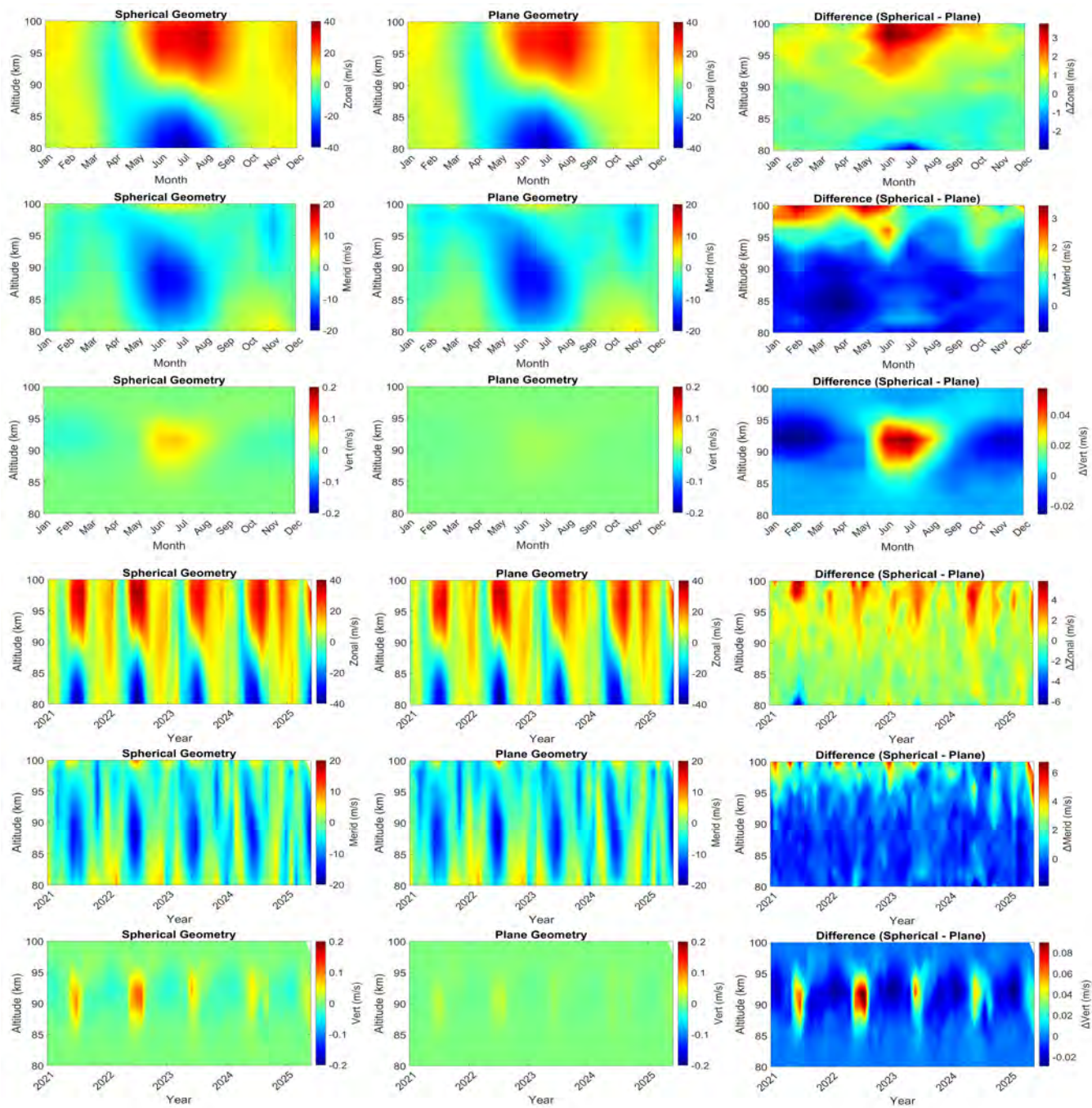


Figure S2. Same as Figure S1, but for a 200 km averaging radius and a 30-minute temporal resolution.

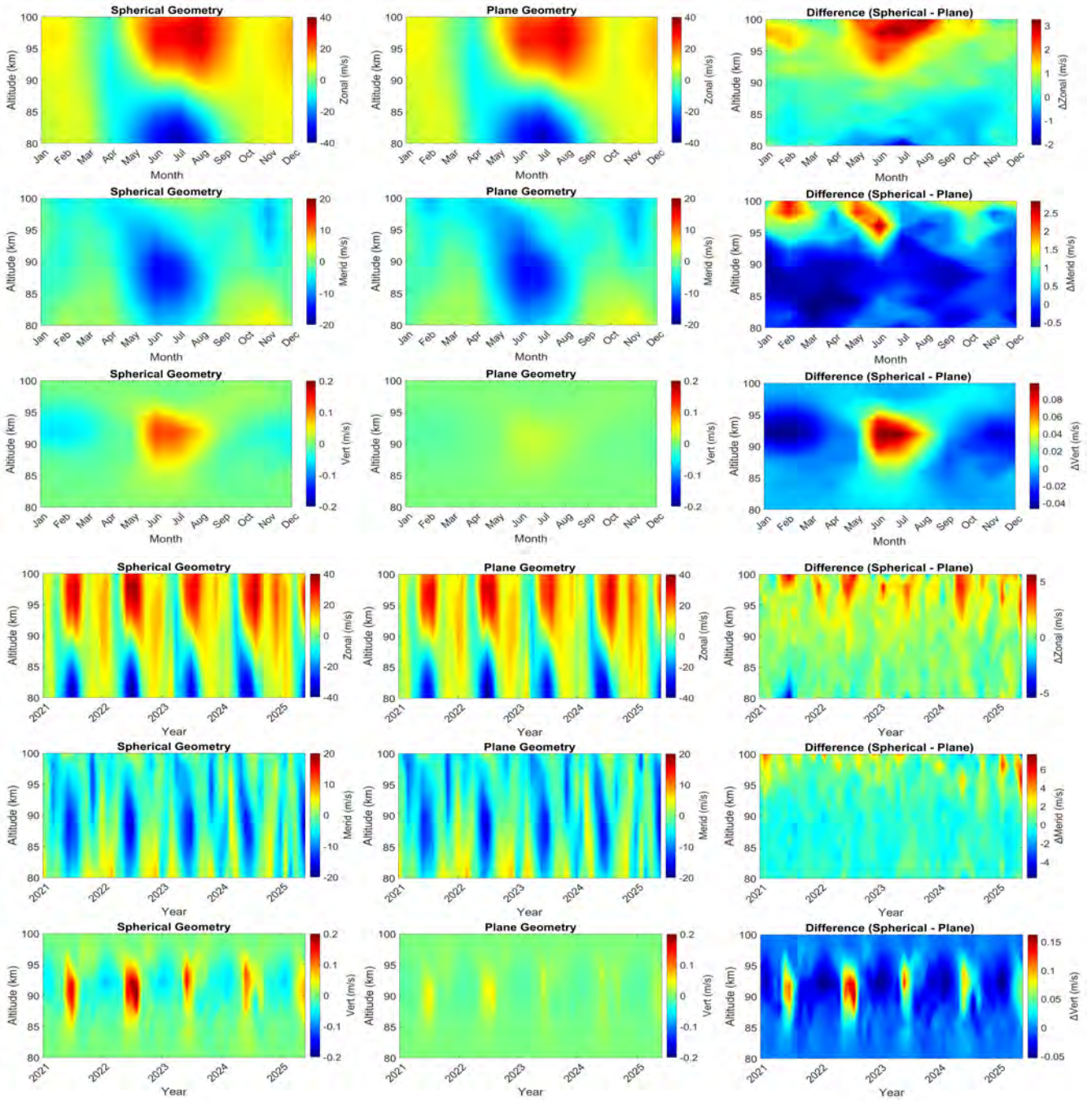


Figure S3. Same as Figure S1, but for a 200 km averaging radius and a 60-minute temporal resolution.

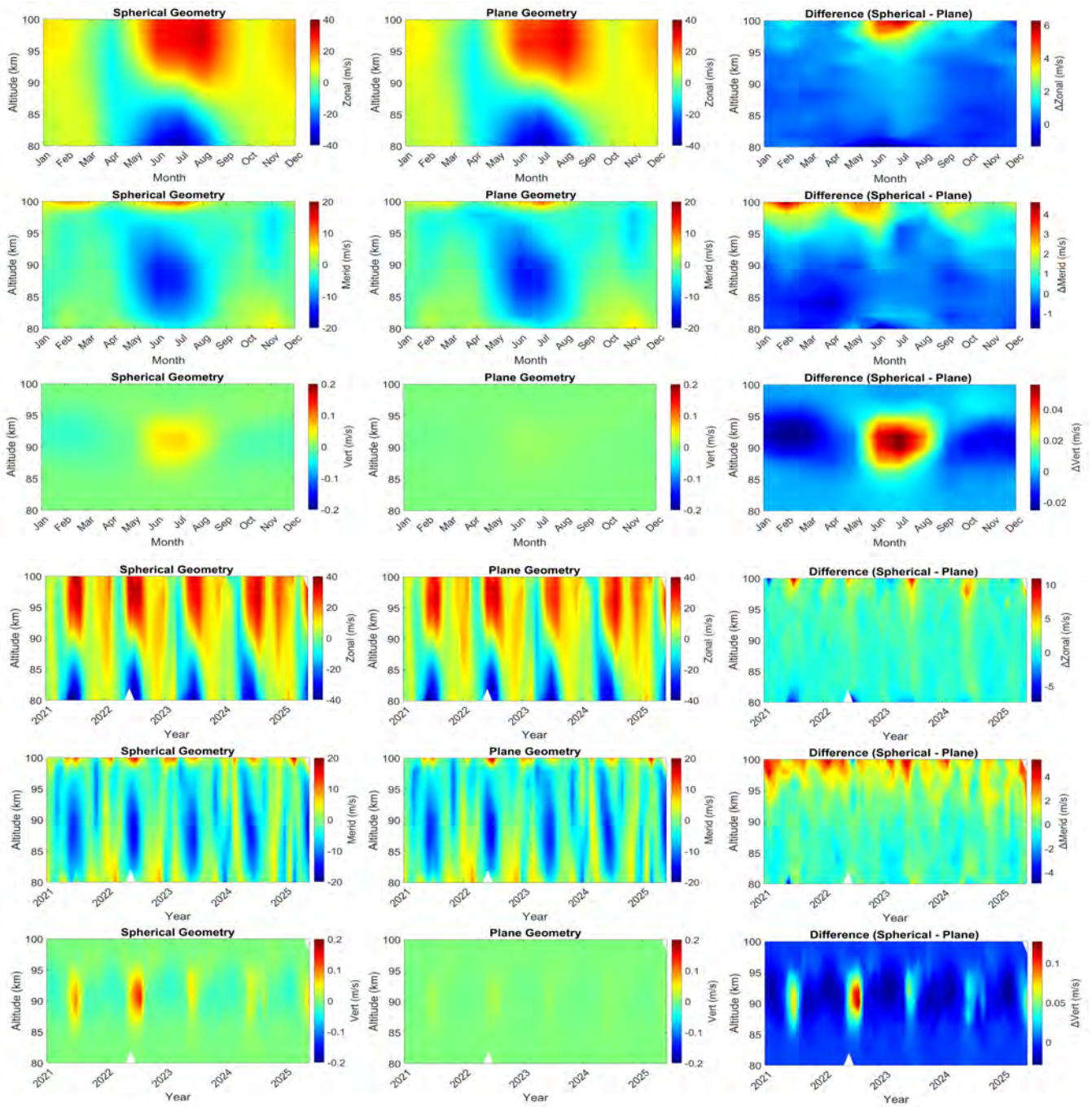


Figure S4. Same as Figure S1, but for a 250 km averaging radius and a 15-minute temporal resolution.

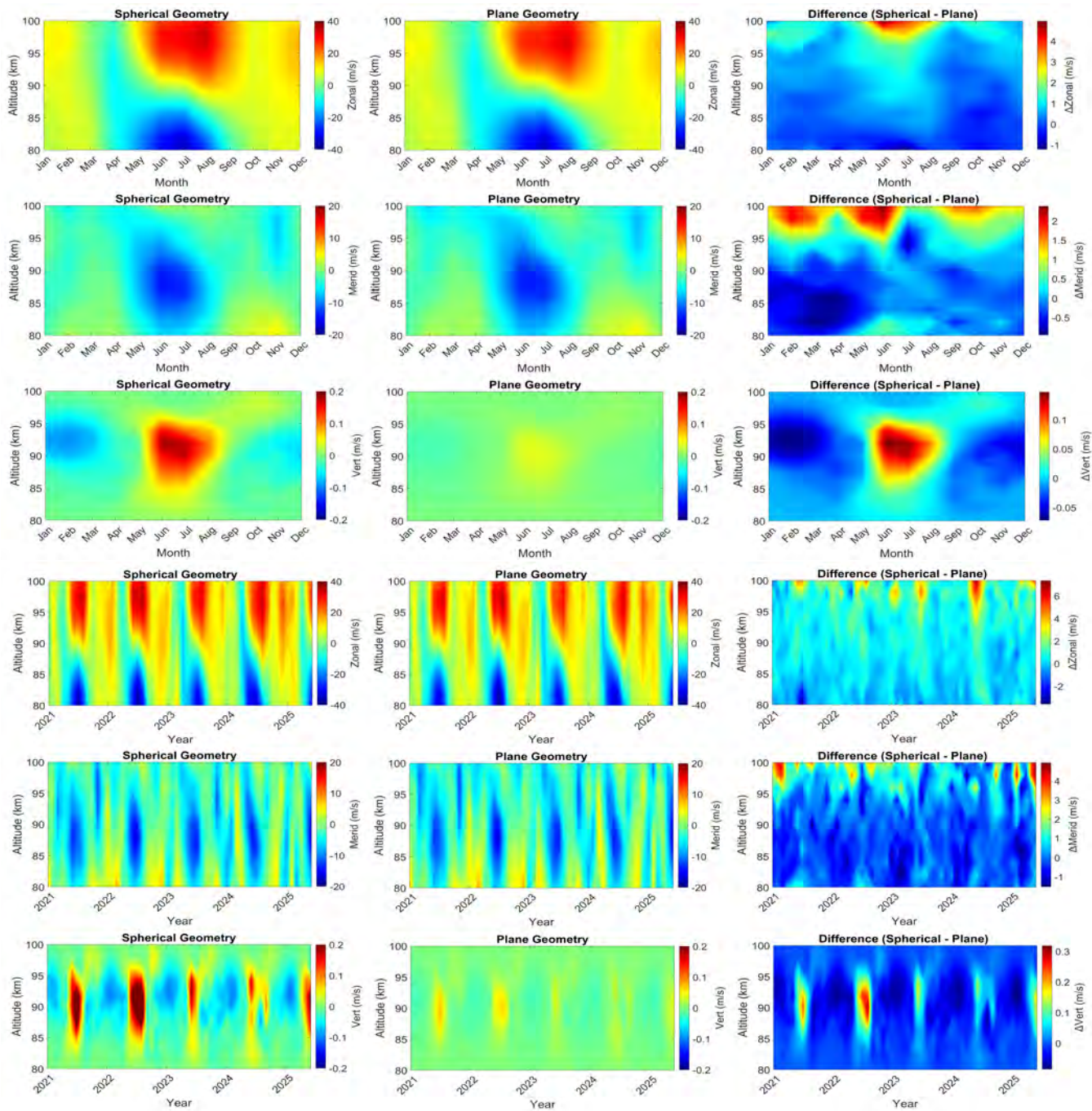


Figure S5. Same as Figure S1, but for a 250 km averaging radius and a 60-minute temporal resolution.

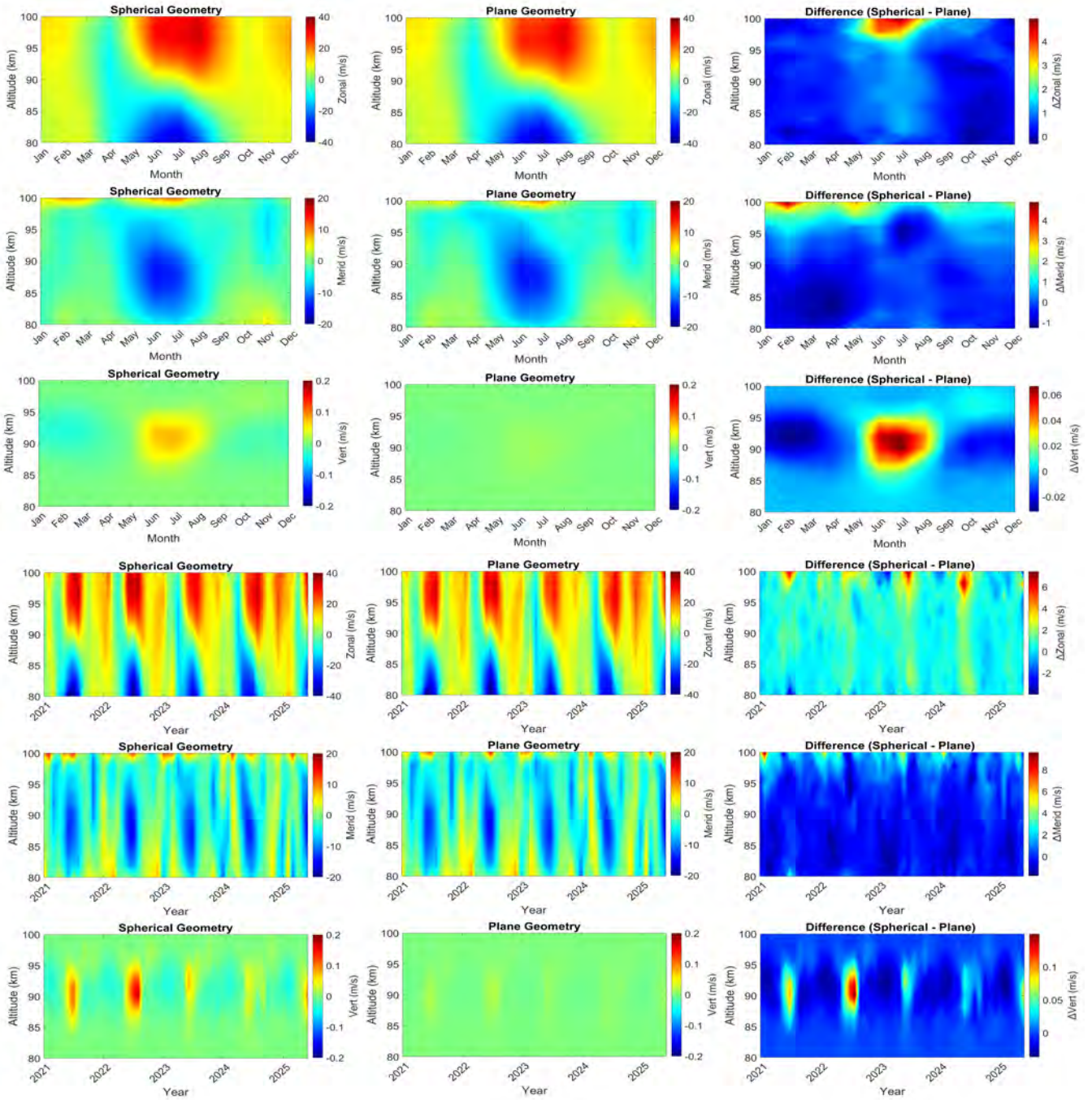


Figure S6. Same as Figure S1, but for a 300 km averaging radius and a 15-minute temporal resolution.

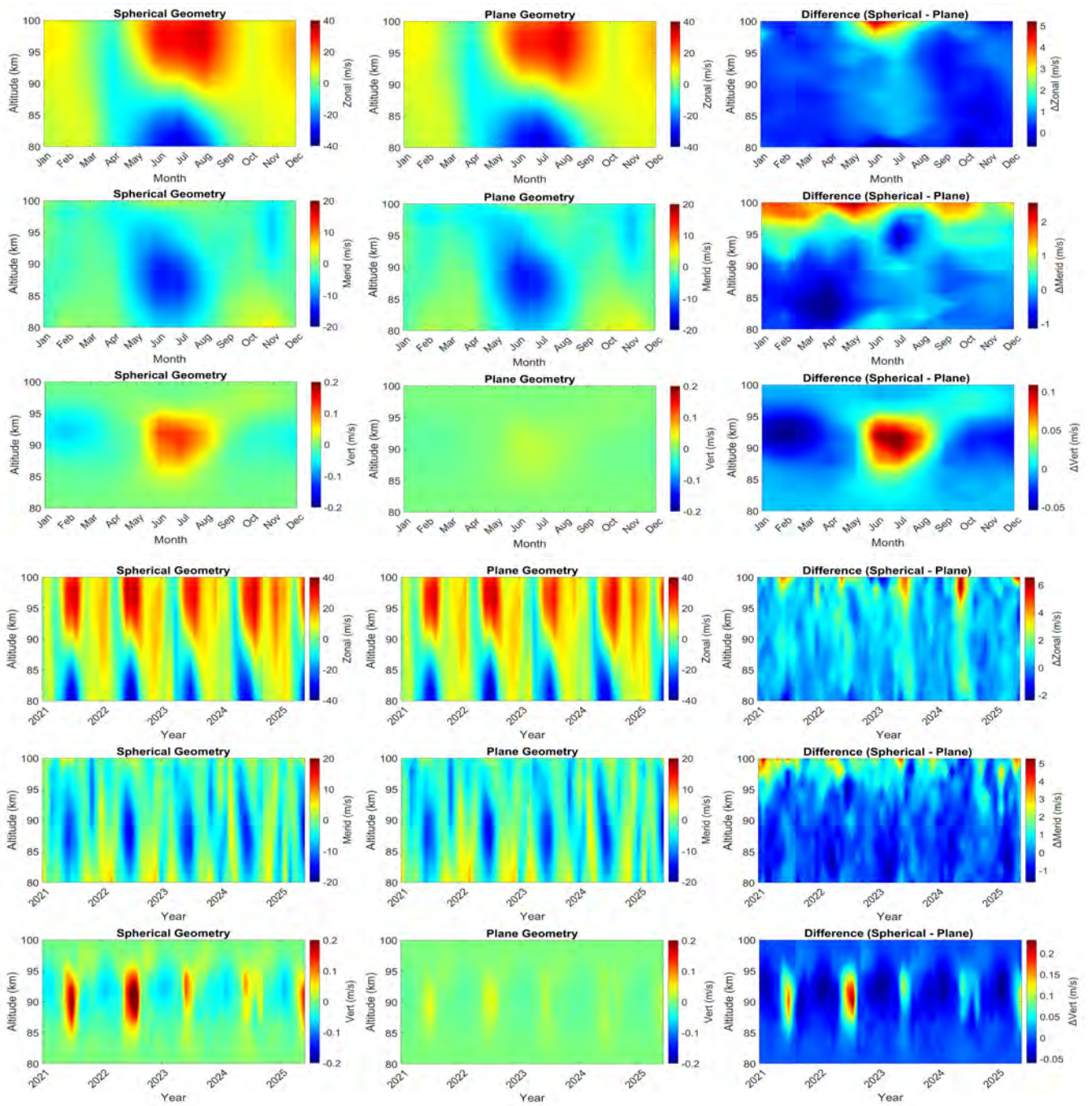


Figure S7. Same as Figure S1, but for a 300 km averaging radius and a 30-minute temporal resolution.

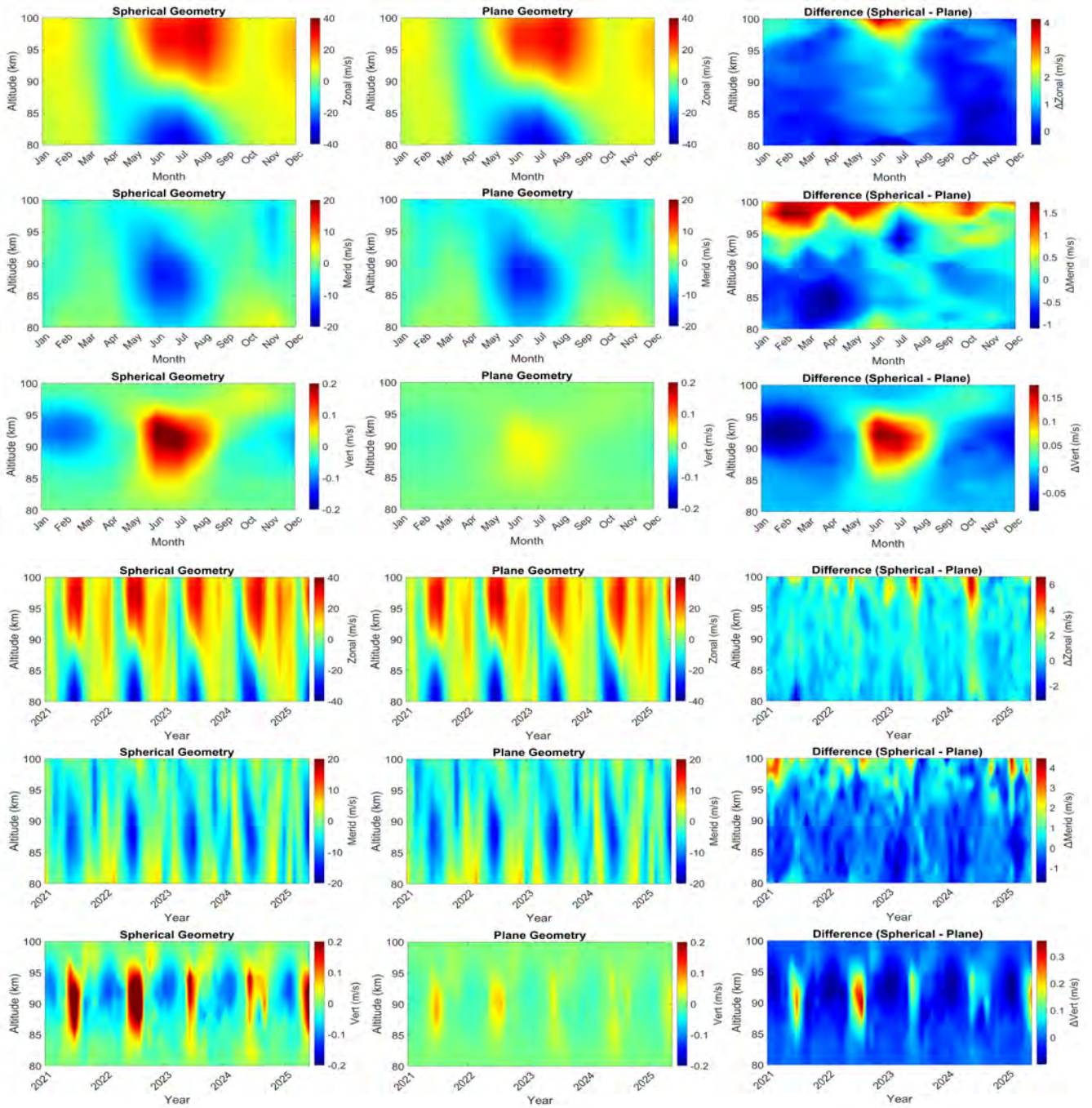


Figure S8. Same as Figure S1, but for a 300 km averaging radius and a 60-minute temporal resolution.

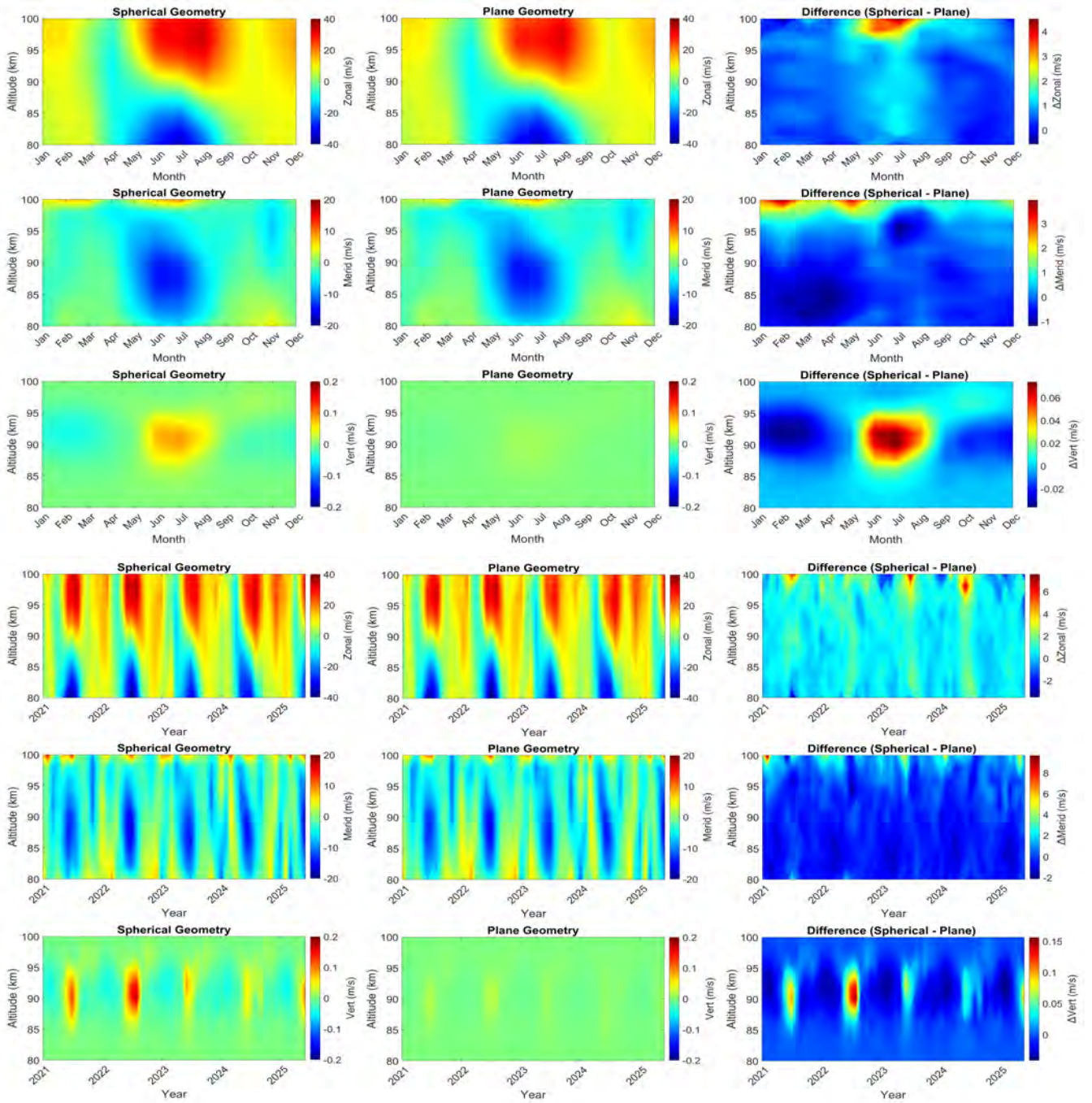


Figure S9. Same as Figure S1, but for a 350 km averaging radius and a 15-minute temporal resolution.

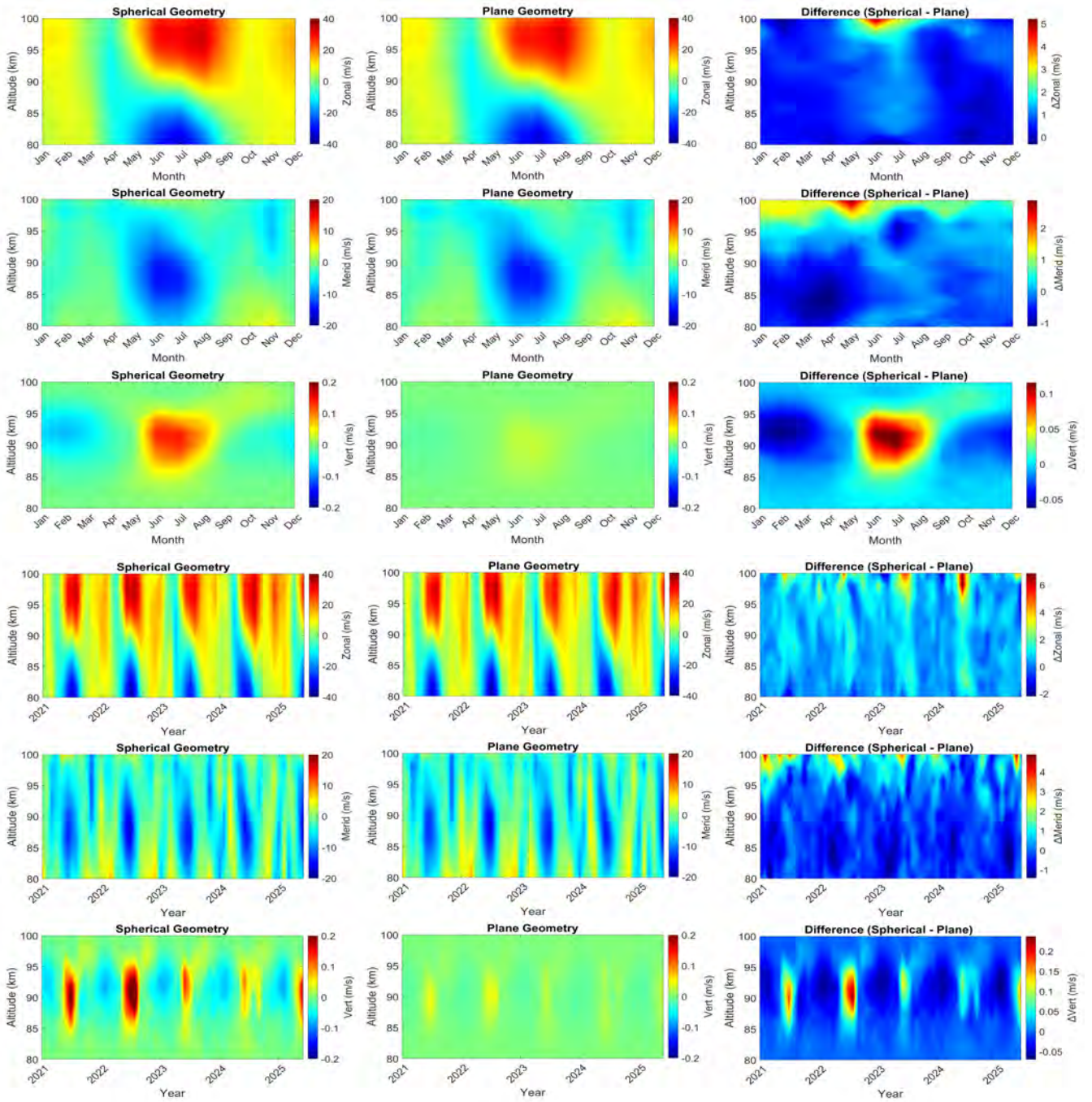


Figure S10. Same as Figure S1, but for a 350 km averaging radius and a 30-minute temporal resolution.

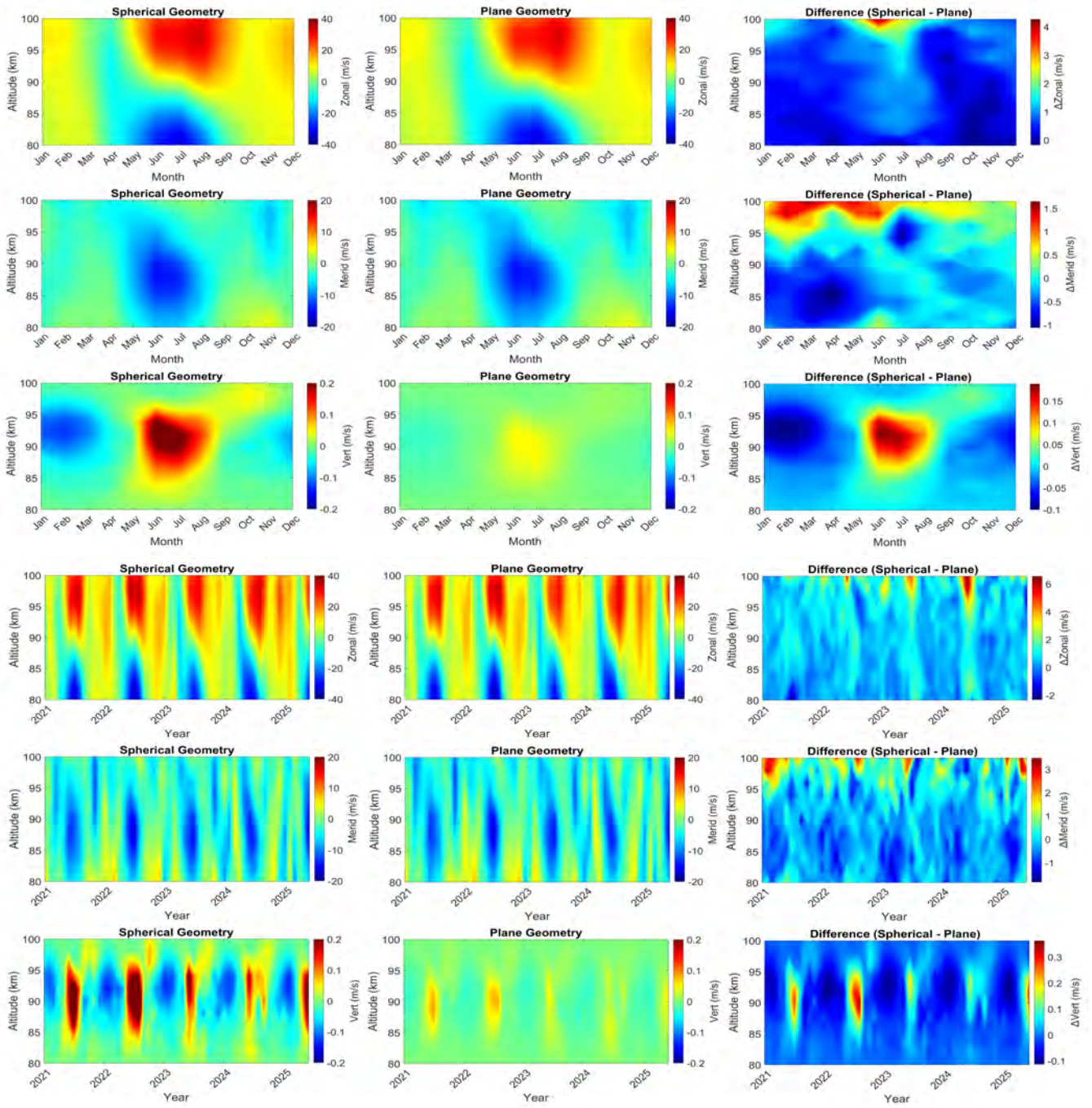


Figure S11. Same as Figure S1, but for a 350 km averaging radius and a 60-minute temporal resolution.

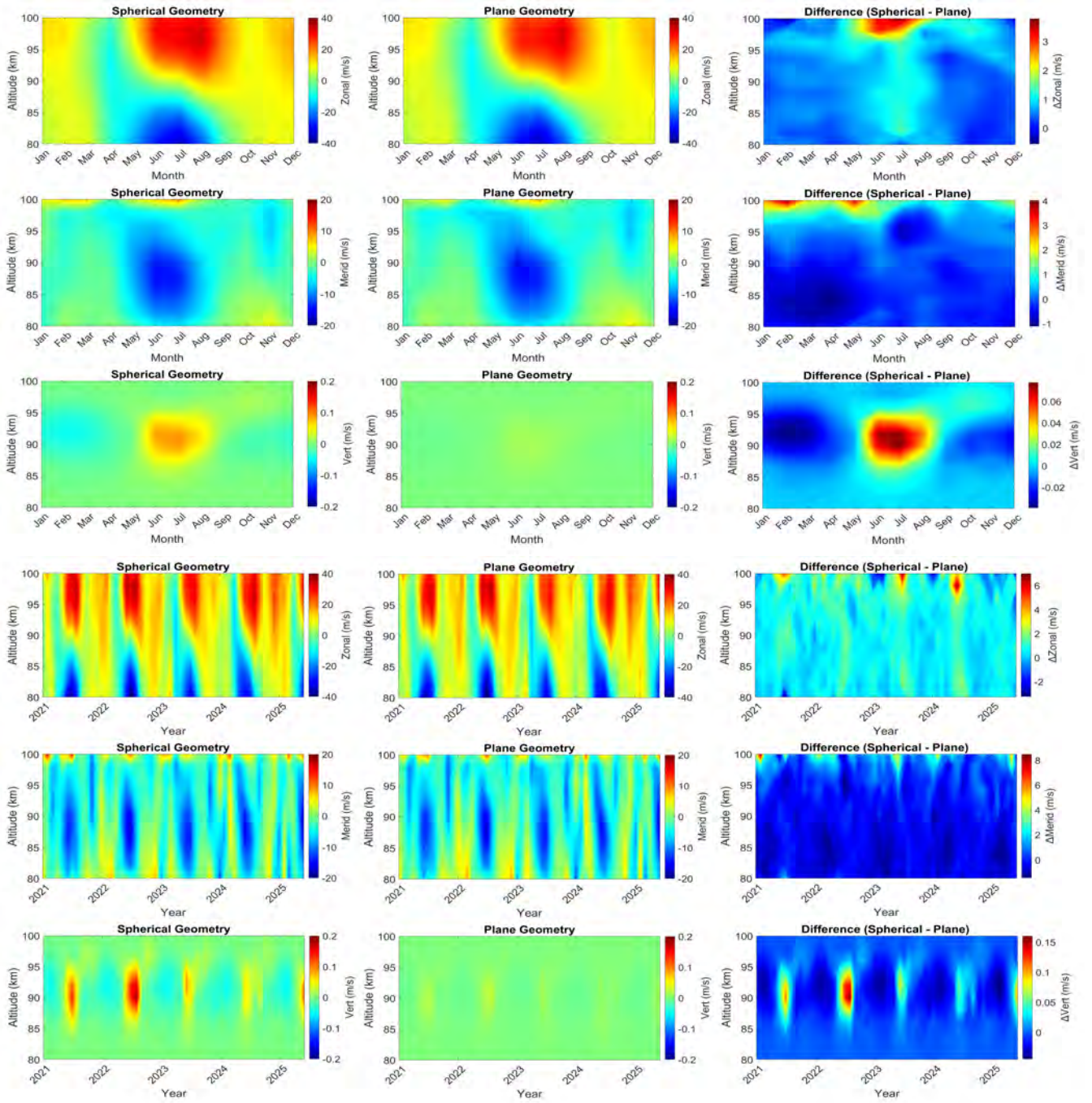


Figure S12. Same as Figure S1, but for a 400 km averaging radius and a 15-minute temporal resolution.

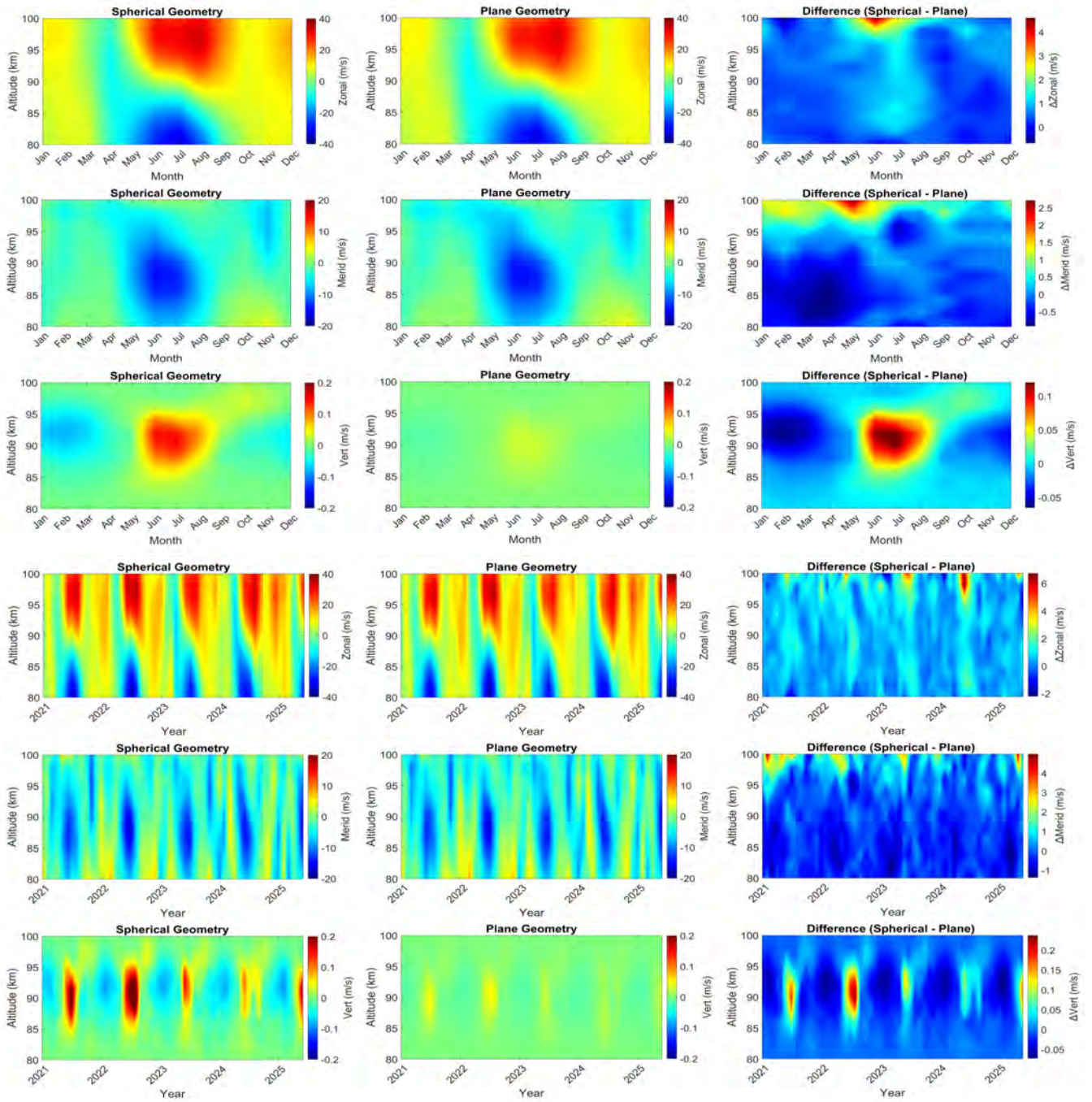


Figure S13. Same as Figure S1, but for a 400 km averaging radius and a 30-minute temporal resolution.

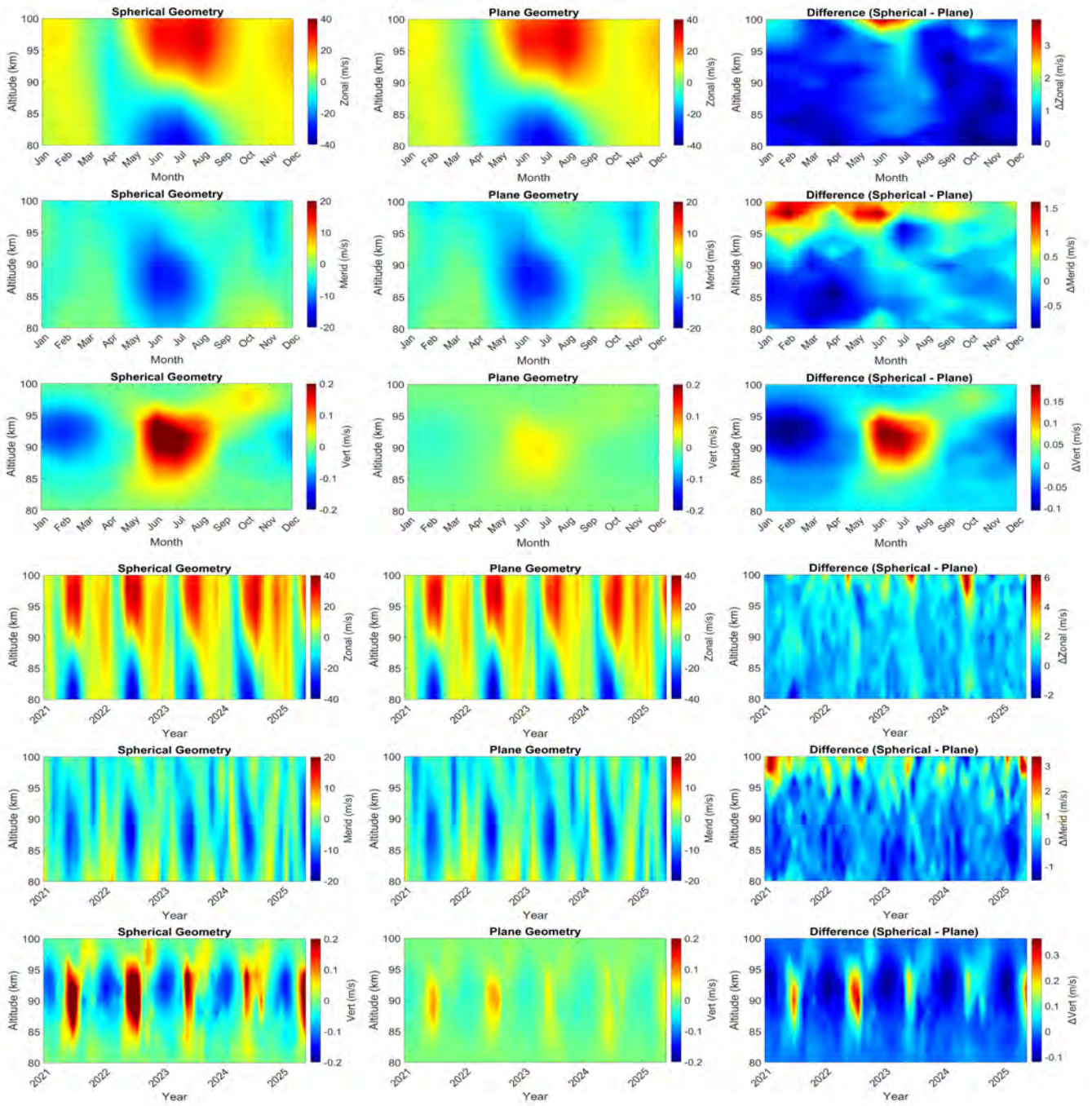


Figure S14. Same as Figure S1, but for a 400 km averaging radius and a 60-minute temporal resolution.

S2 Composite of the Higher-order Kinematic Variables Derived from SVVP Retrieval

This section presents the climatological mean state of the higher-order kinematic variables, including the horizontal divergence, shearing deformation, stretching deformation, and the relative vorticity retrieved using the SVVP algorithm (spherical geometry) and the conventional VVP (plane geometry). These figures illustrate the seasonal wind climatology for all the variables in both geometries, along with their differences, similar to those in figures 7 and 8, but for averaging radii of 200, 250, 300, 350, and 400 km at temporal resolutions of 15, 30, and 60 minutes.

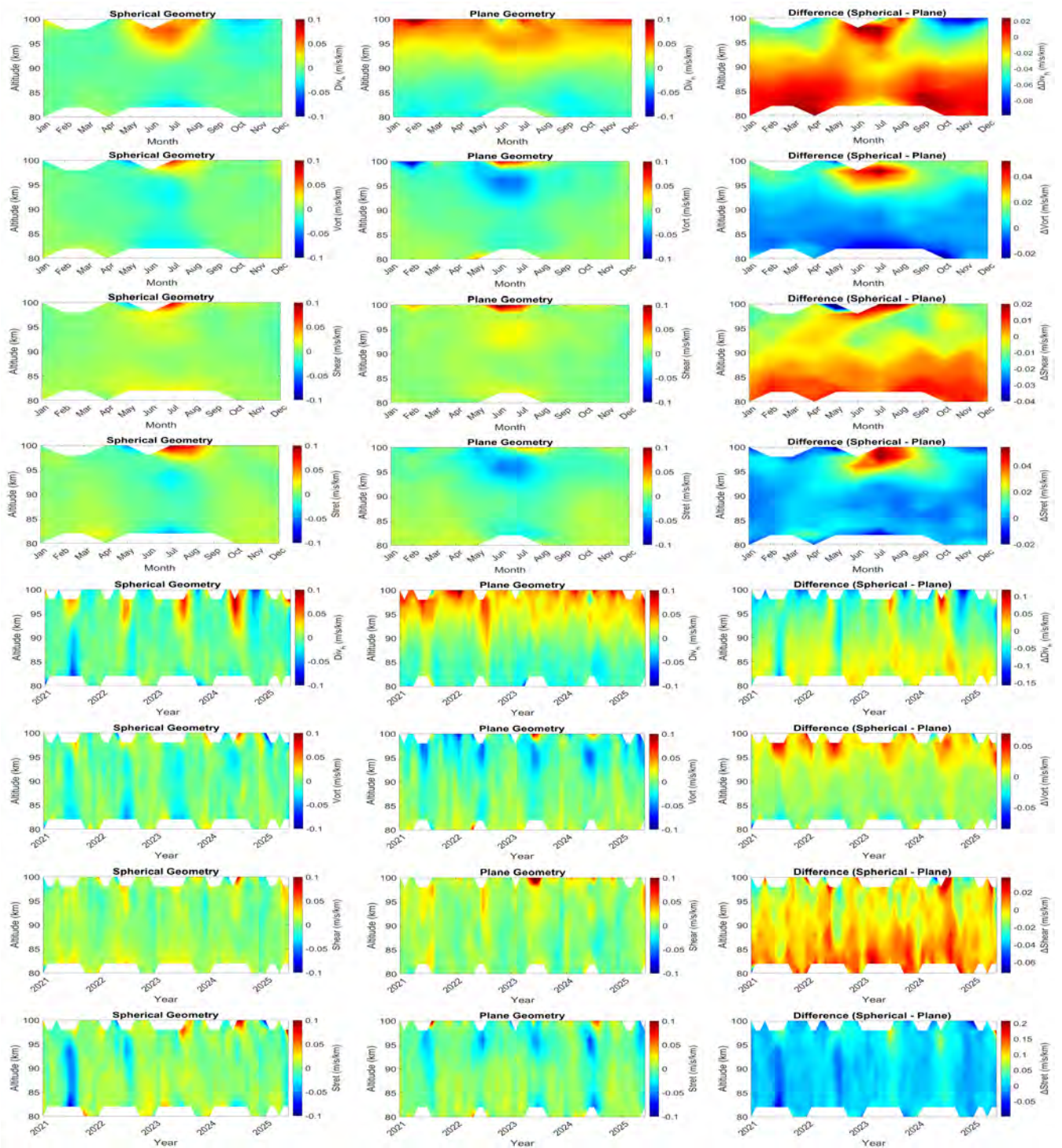


Figure S15. Composites of horizontal divergence, shearing deformation, stretching deformation, and relative vorticity using Volume Velocity Processing (VVP) with 200 km averaging radius and 15-minute resolution. The first three rows show the monthly mean results; the remaining rows display seasonal averages. Each panel compares spherical geometry, plane geometry, and their differences.

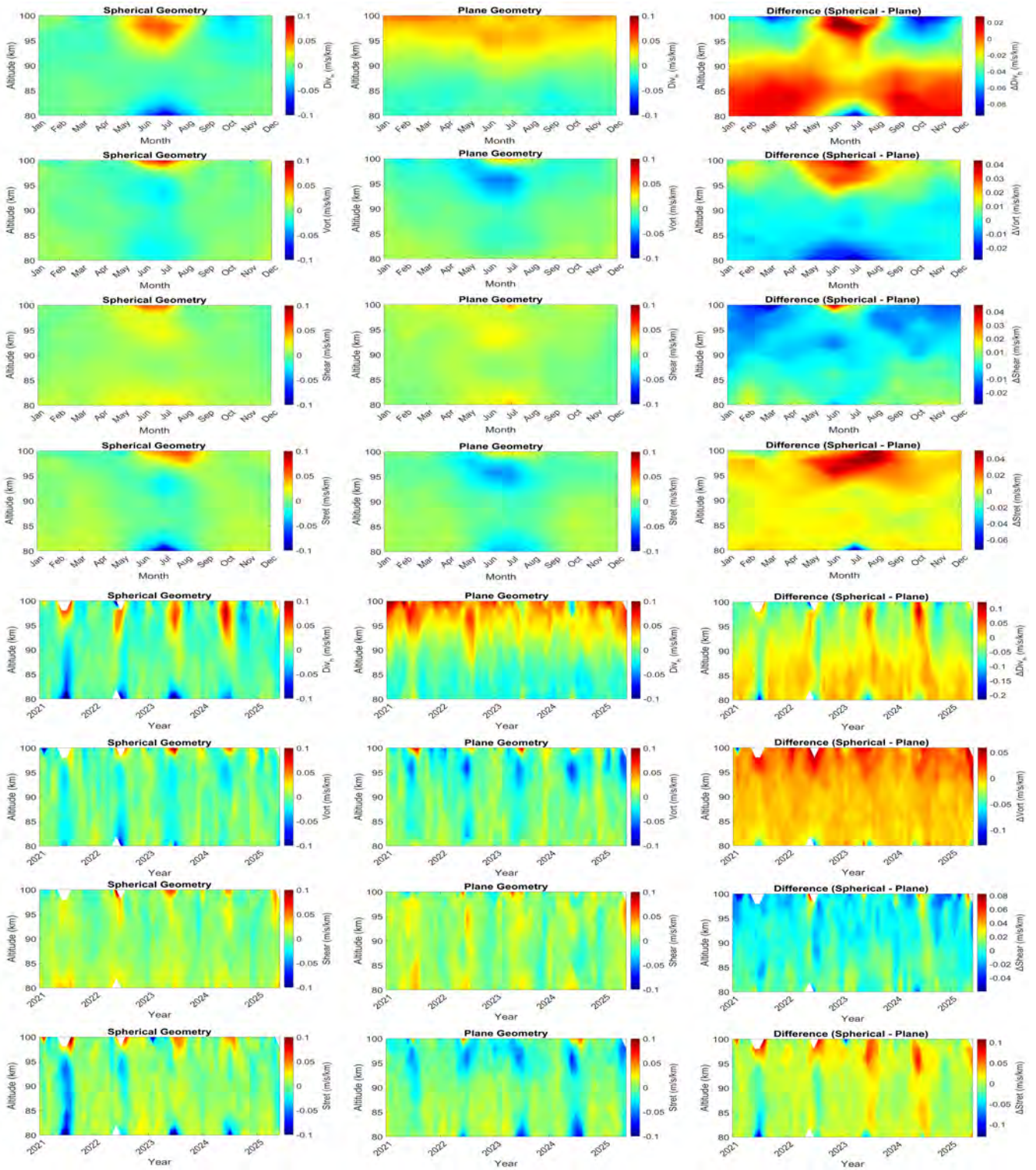


Figure S16. Same as Figure S15, but for a 200 km averaging radius and a 30-minute temporal resolution.

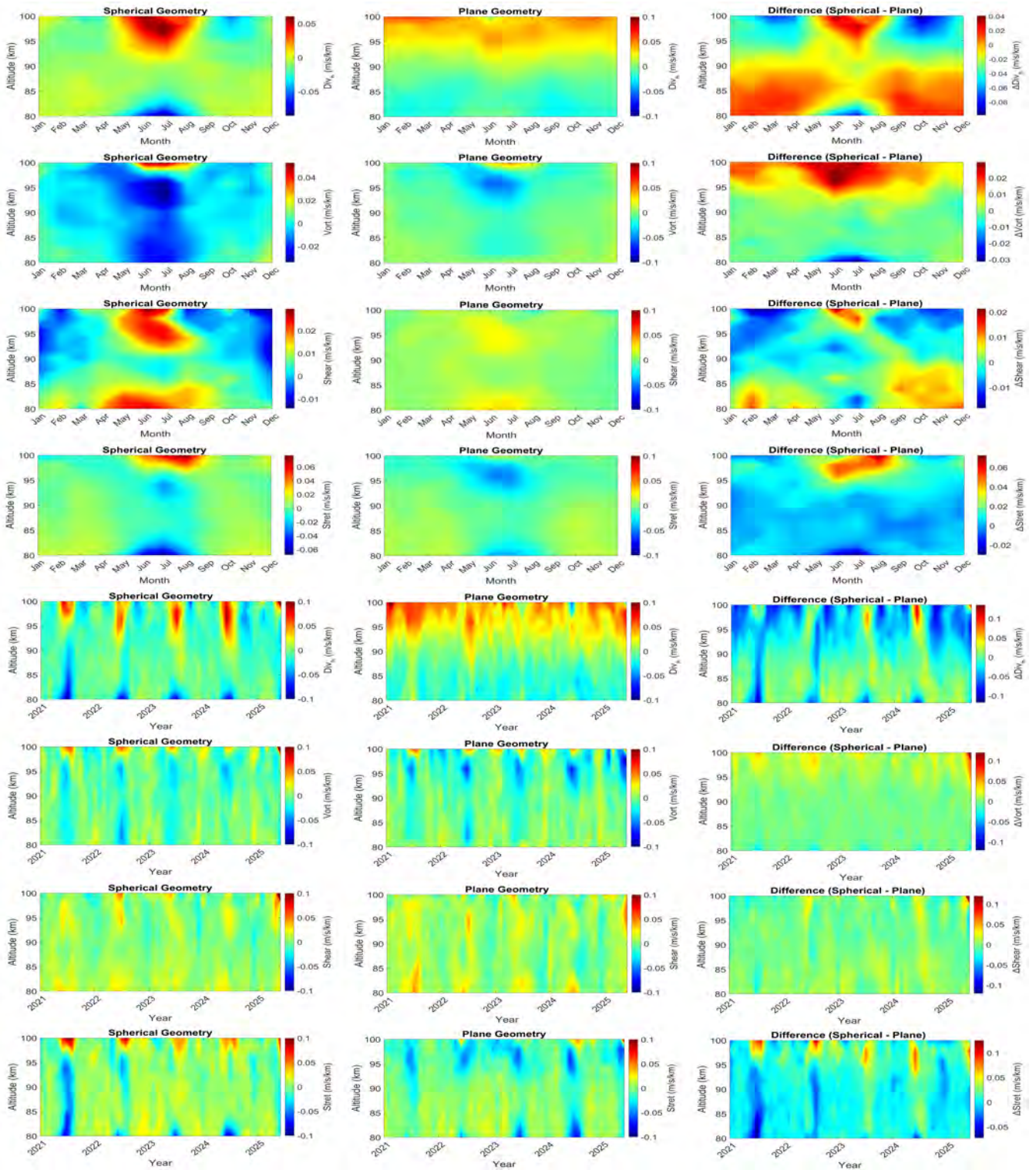


Figure S17. Same as Figure S15, but for a 200 km averaging radius and a 60-minute temporal resolution.

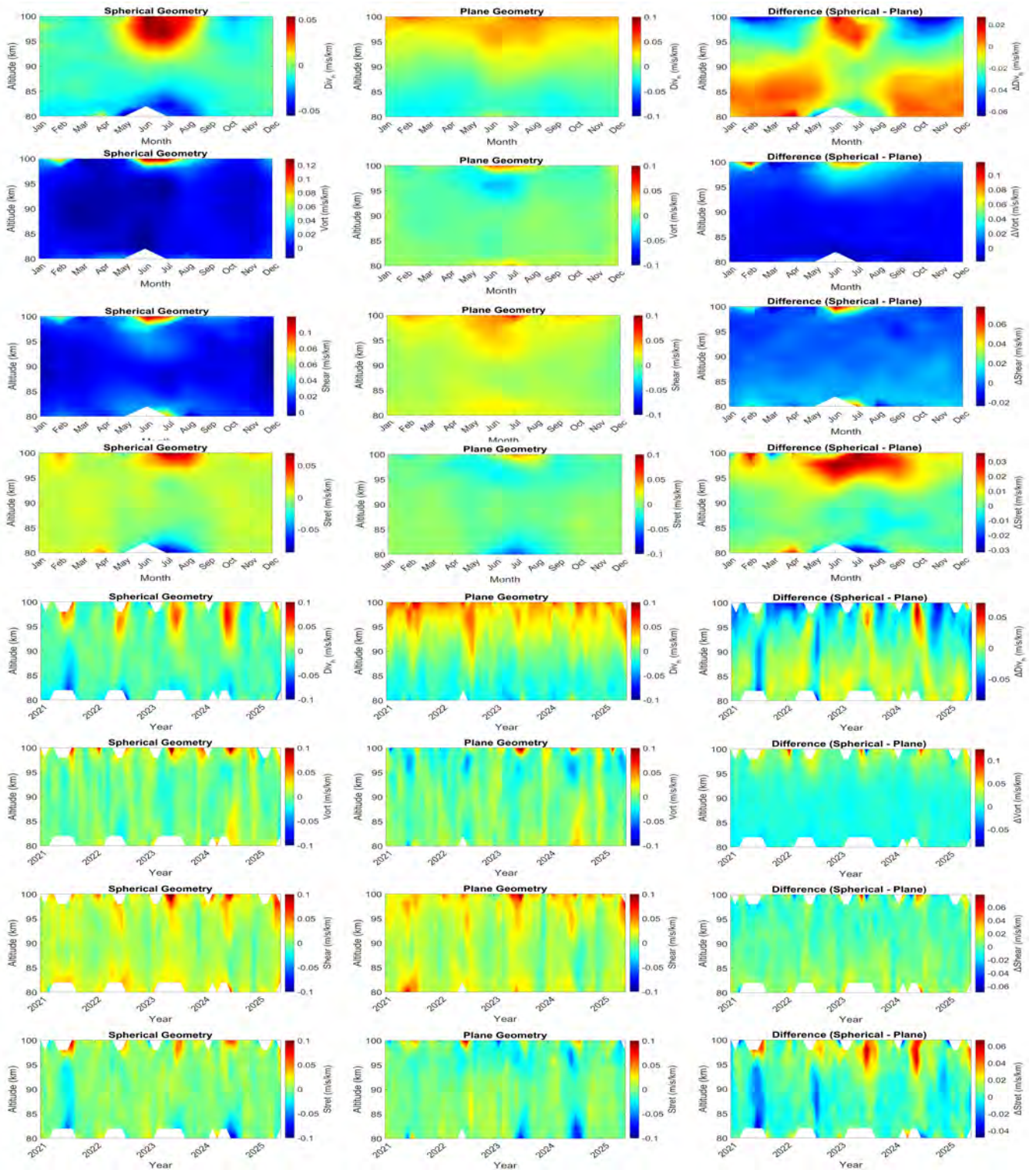


Figure S18. Same as Figure S15, but for a 250 km averaging radius and a 15-minute temporal resolution.

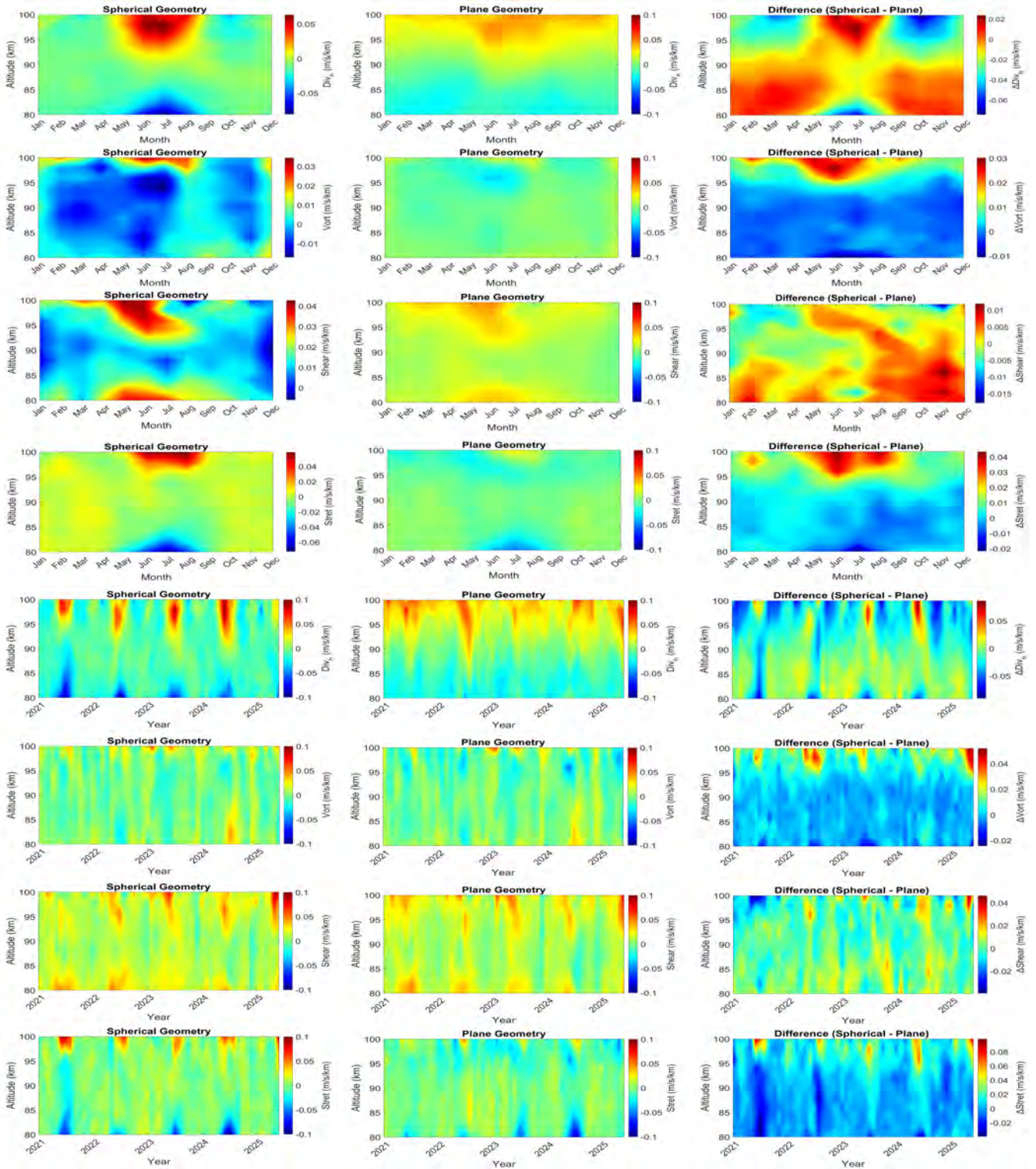


Figure S19. Same as Figure S15, but for a 250 km averaging radius and a 60-minute temporal resolution.

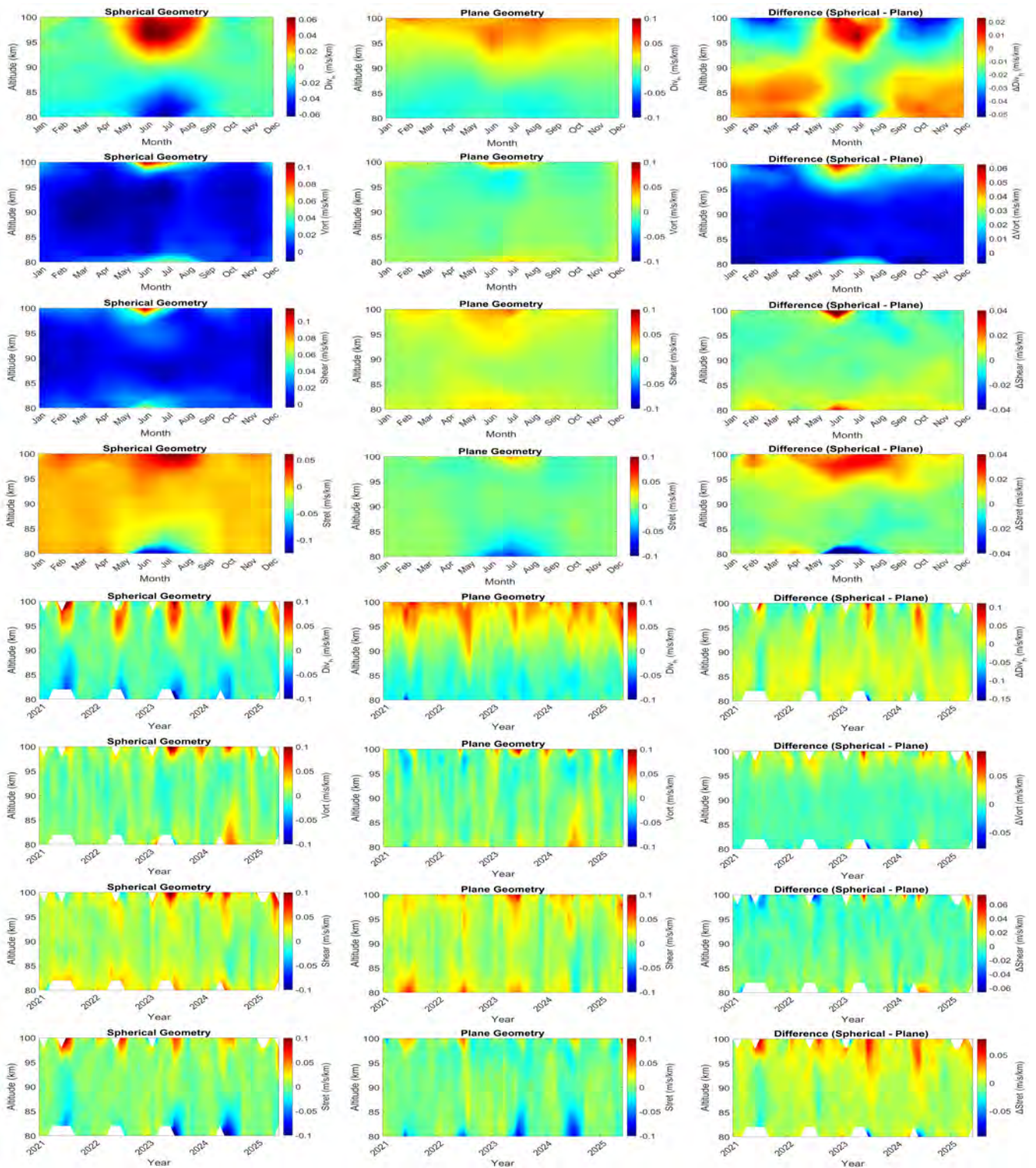


Figure S20. Same as Figure S15, but for a 300 km averaging radius and a 15-minute temporal resolution.

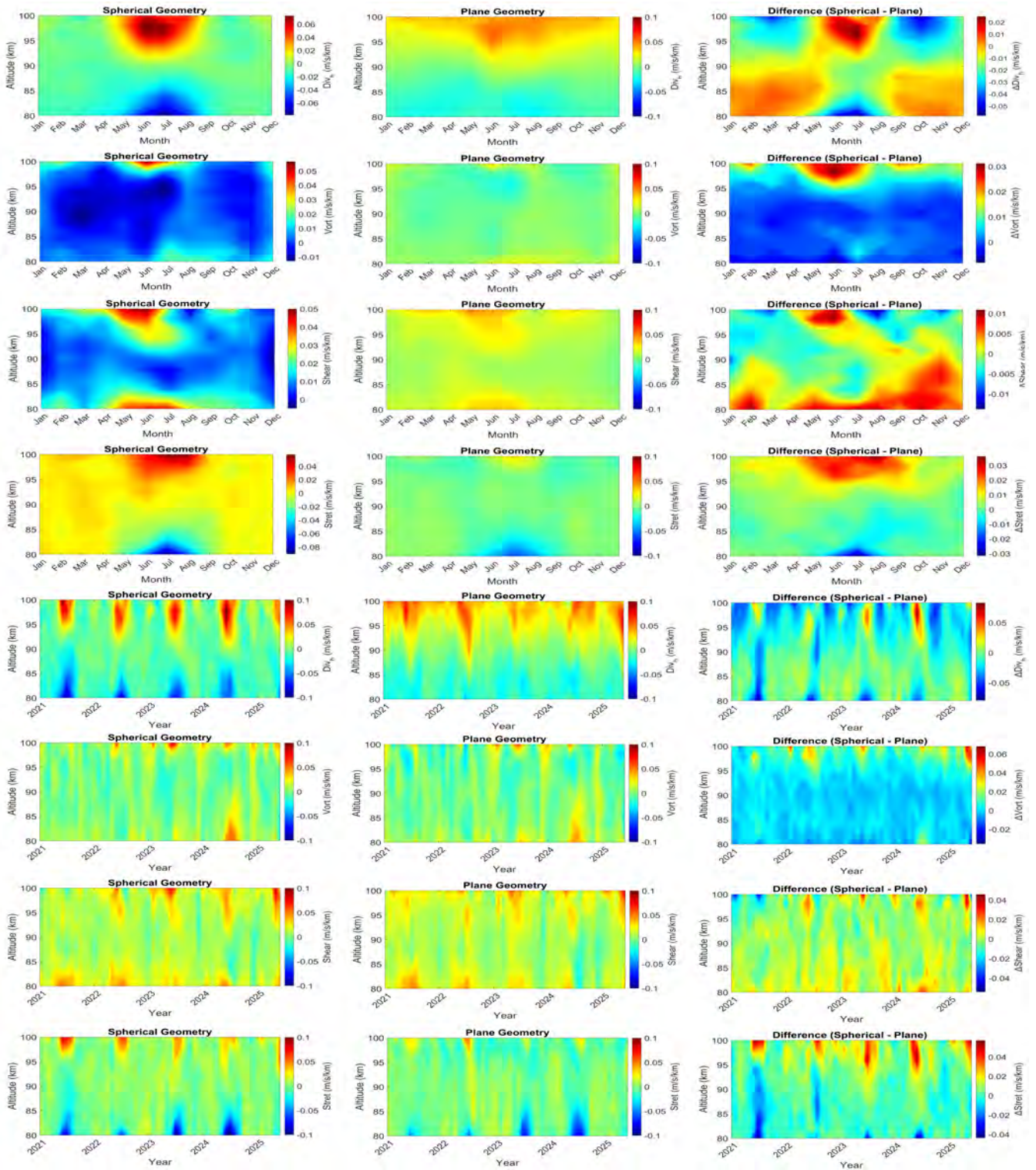


Figure S21. Same as Figure S15, but for a 300 km averaging radius and a 30-minute temporal resolution.

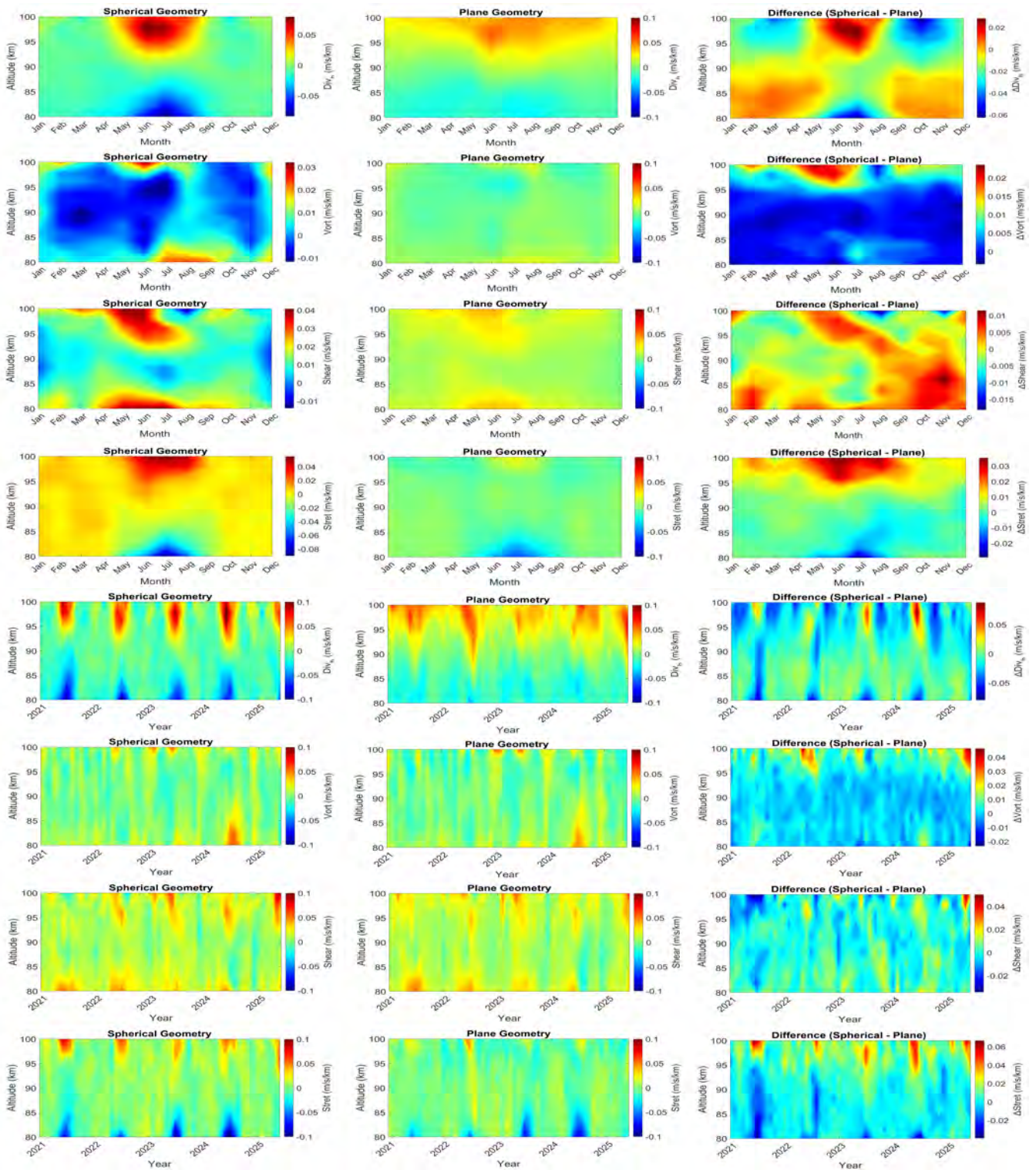


Figure S22. Same as Figure S15, but for a 300 km averaging radius and a 60-minute temporal resolution.

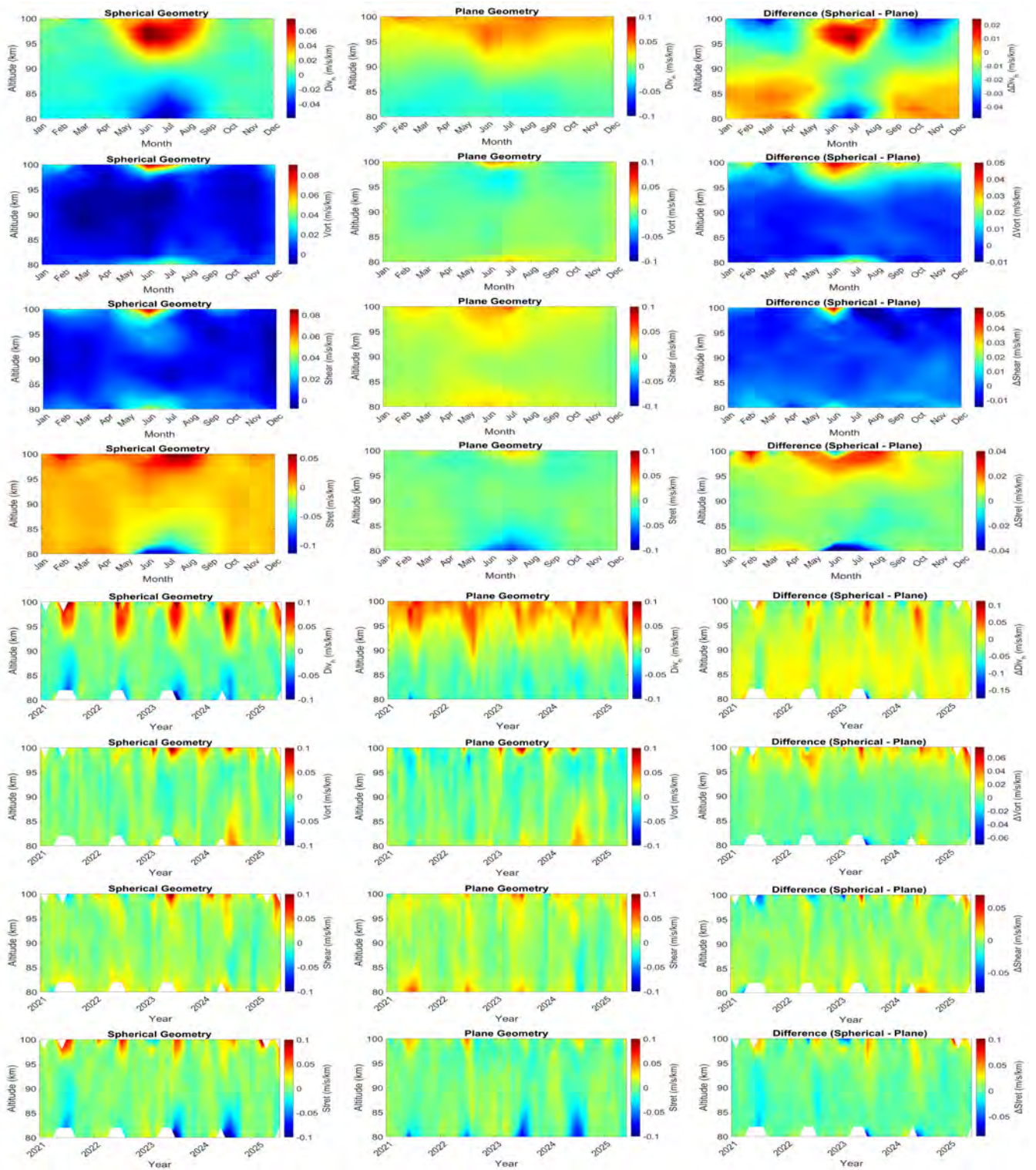


Figure S23. Same as Figure S15, but for a 350 km averaging radius and a 15-minute temporal resolution.

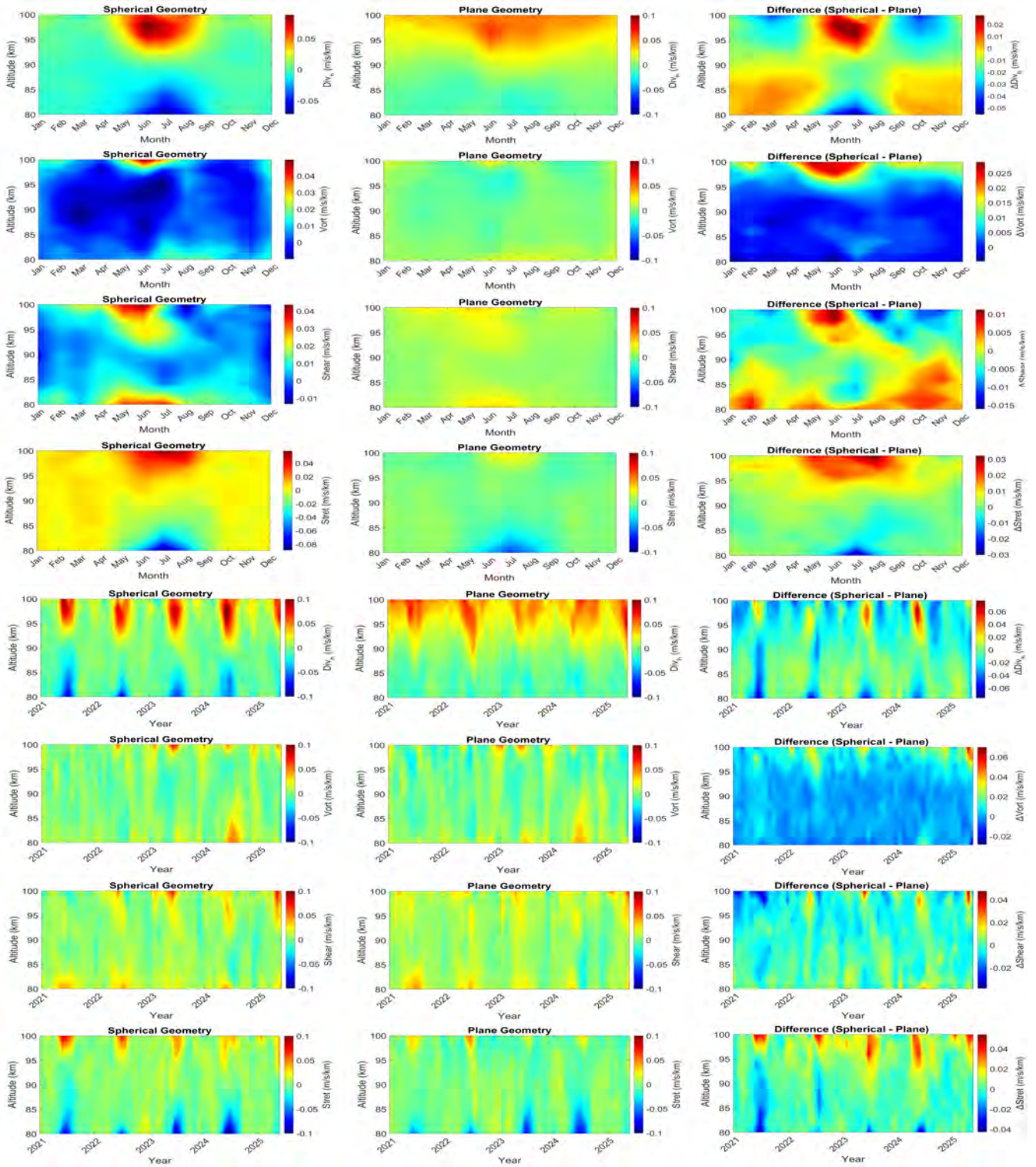


Figure S24. Same as Figure S15, but for a 350 km averaging radius and a 30-minute temporal resolution.

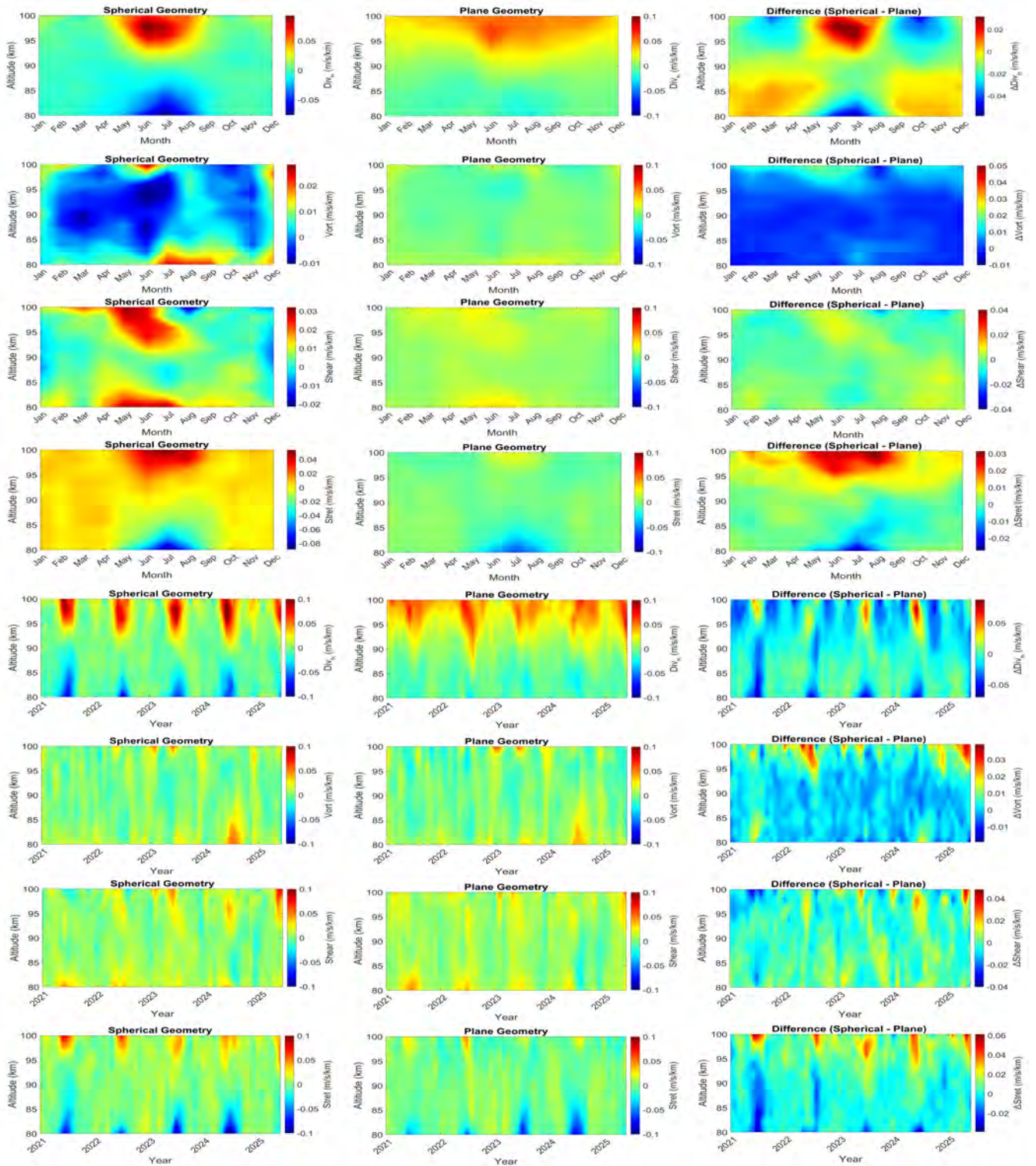


Figure S25. Same as Figure S15, but for a 350 km averaging radius and a 60-minute temporal resolution.

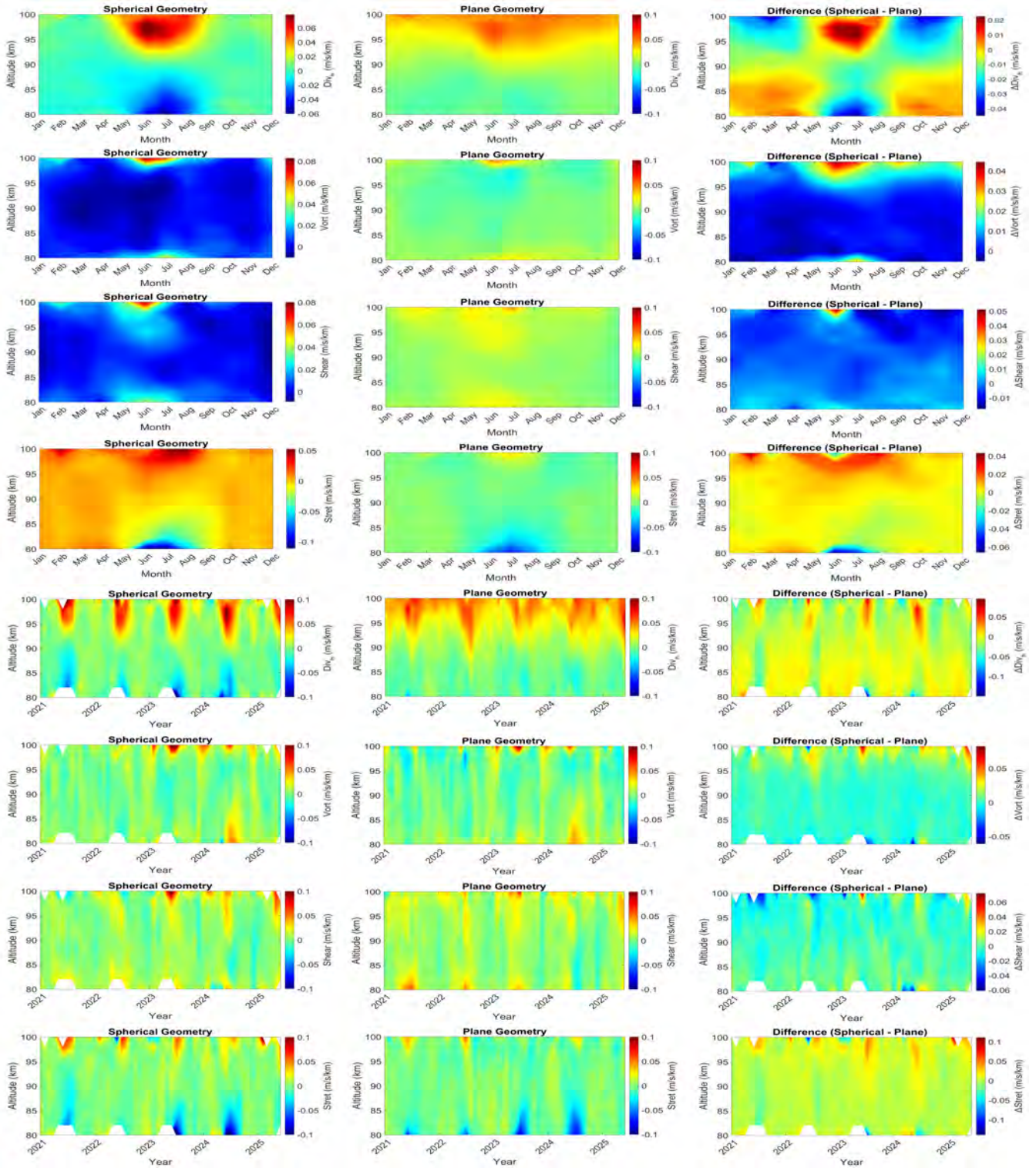


Figure S26. Same as Figure S15, but for a 400 km averaging radius and a 15-minute temporal resolution.

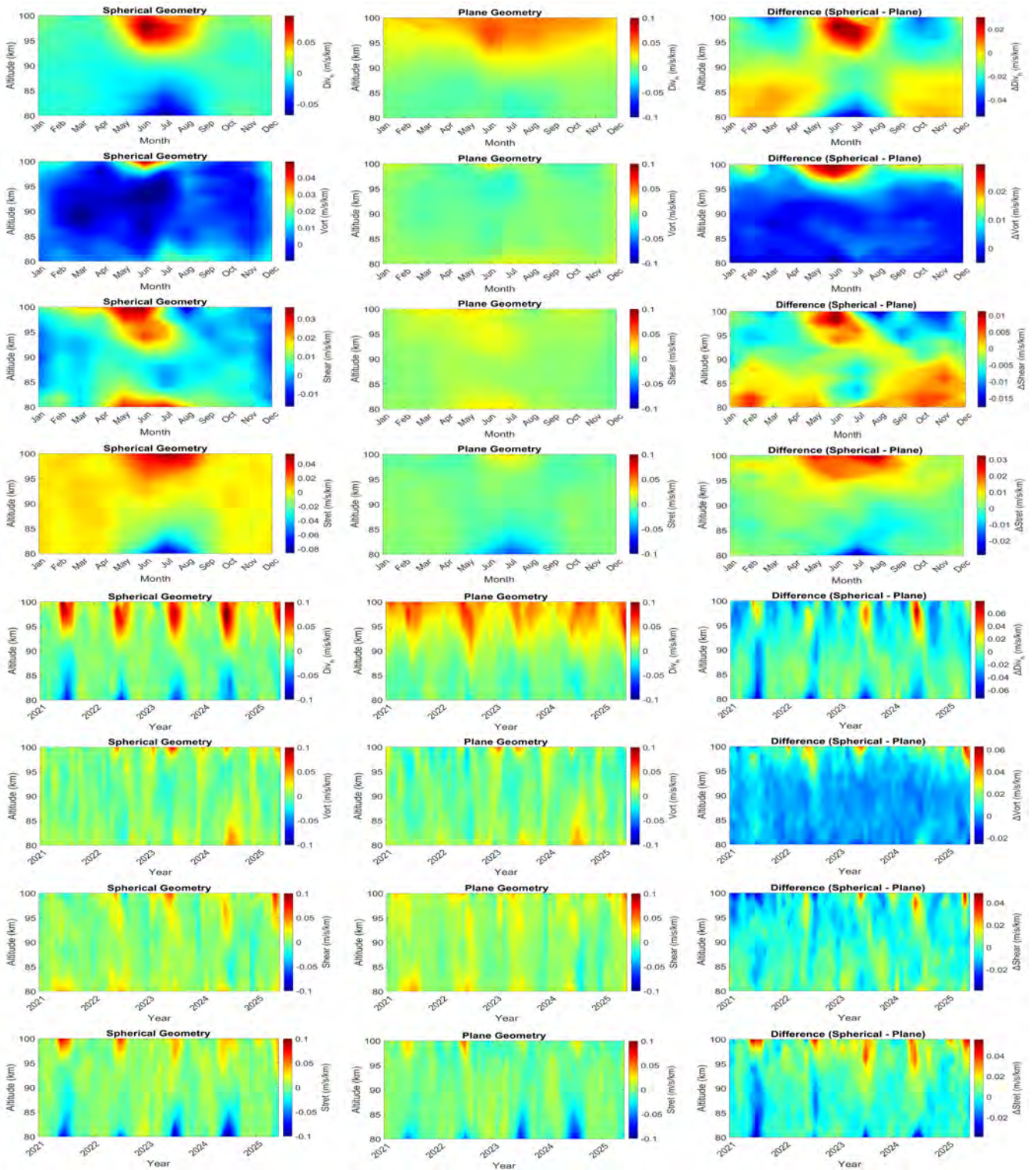


Figure S27. Same as Figure S15, but for a 400 km averaging radius and a 30-minute temporal resolution.

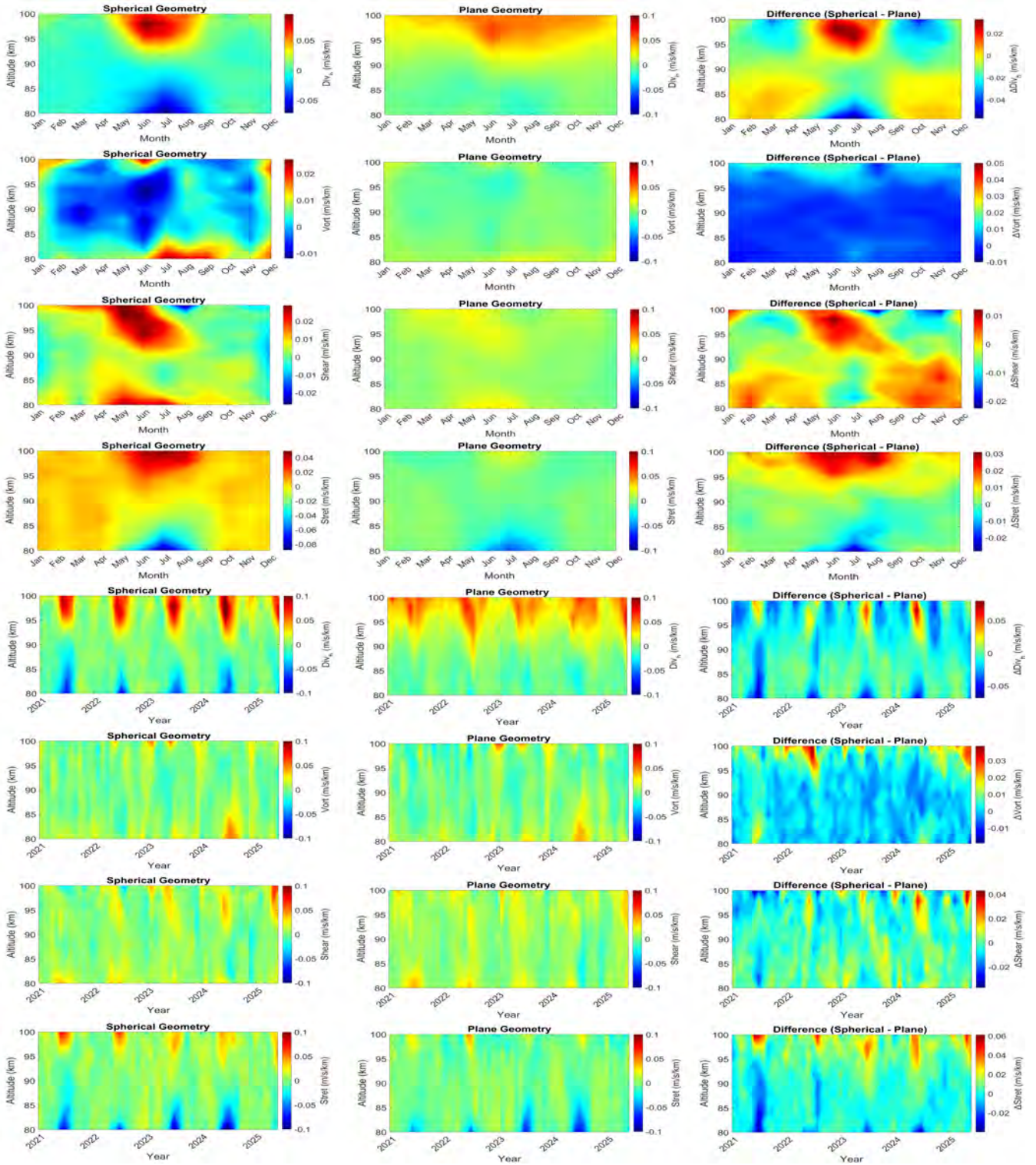


Figure S28. Same as Figure S15, but for a 400 km averaging radius and a 60-minute temporal resolution.

In this section, we compare Volume Velocity Processing (VVP) retrievals using spherical and plane geometries across averaging radii of 200, 300, 350, and 400 km at temporal resolutions of 15, 30, and 60 minutes. Results for a 250 km averaging radius at 15 and 60 minutes are also included.

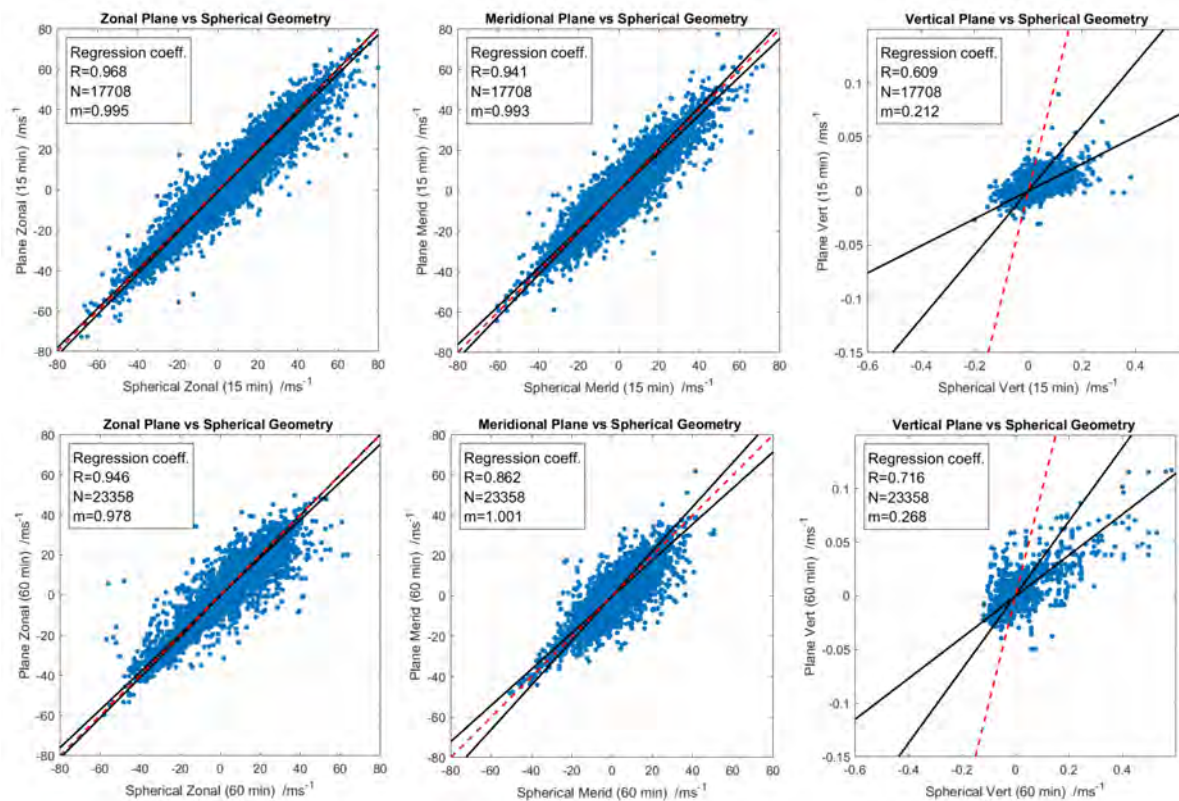


Figure S29. Correlation between the spherical and plane geometry retrieved zonal, meridional, and vertical wind components using Volume Velocity Processing (VVP) for a 250 km averaging radius. Panels correspond to temporal resolutions of 15 (first panel), 30 (in the main manuscript), and 60 minutes (second panel). The top row compares 15-minute and 30-minute temporal resolutions, while the bottom row compares 60-minute and 30-minute temporal resolutions. Each panel presents daily mean scatter points, robust regression fits (black solid line), 1:1 reference lines (red dashed), and annotated statistics (correlation coefficient (R), sample size (N), and the slope (m)).

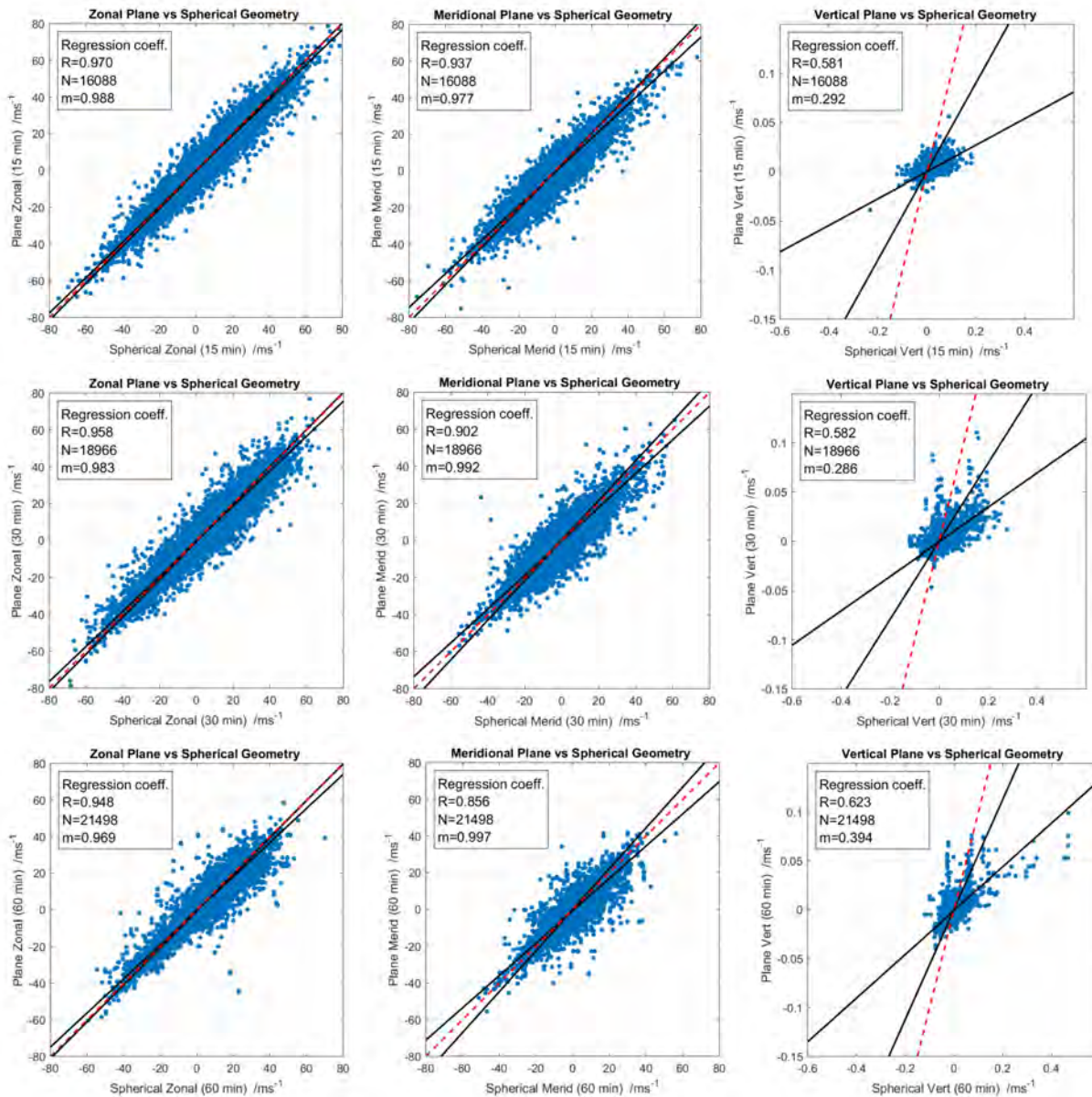


Figure S30. Same as Figure S29, but for a 200 km averaging radius and a temporal resolution of 15 (first panel), 30 (second panel), and 60 (third panel) minutes.

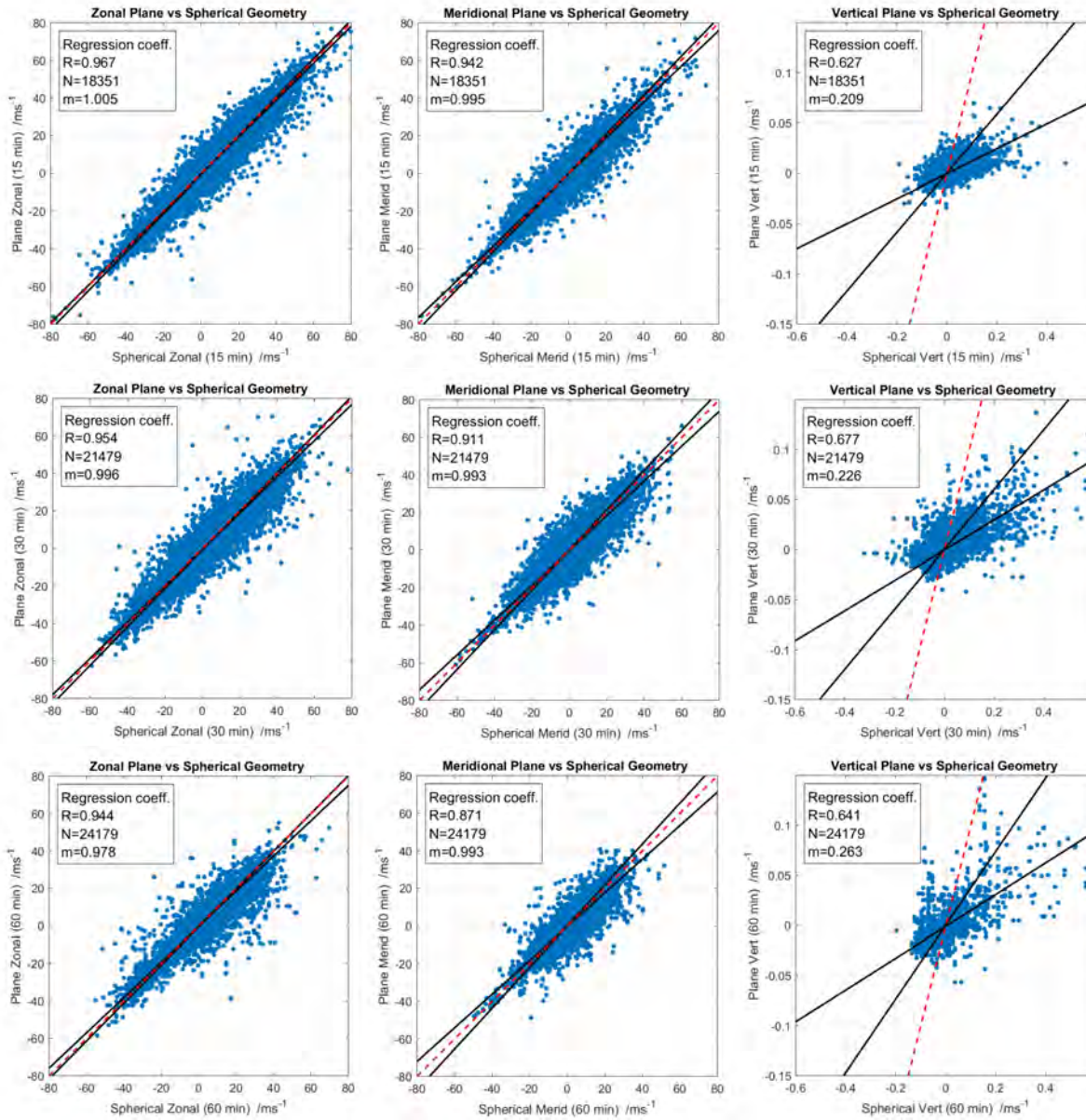


Figure S31. Same as Figure S29, but for a 300 km averaging radius and a temporal resolution of 15 (first panel), 30 (second panel), and 60 (third panel) minutes.

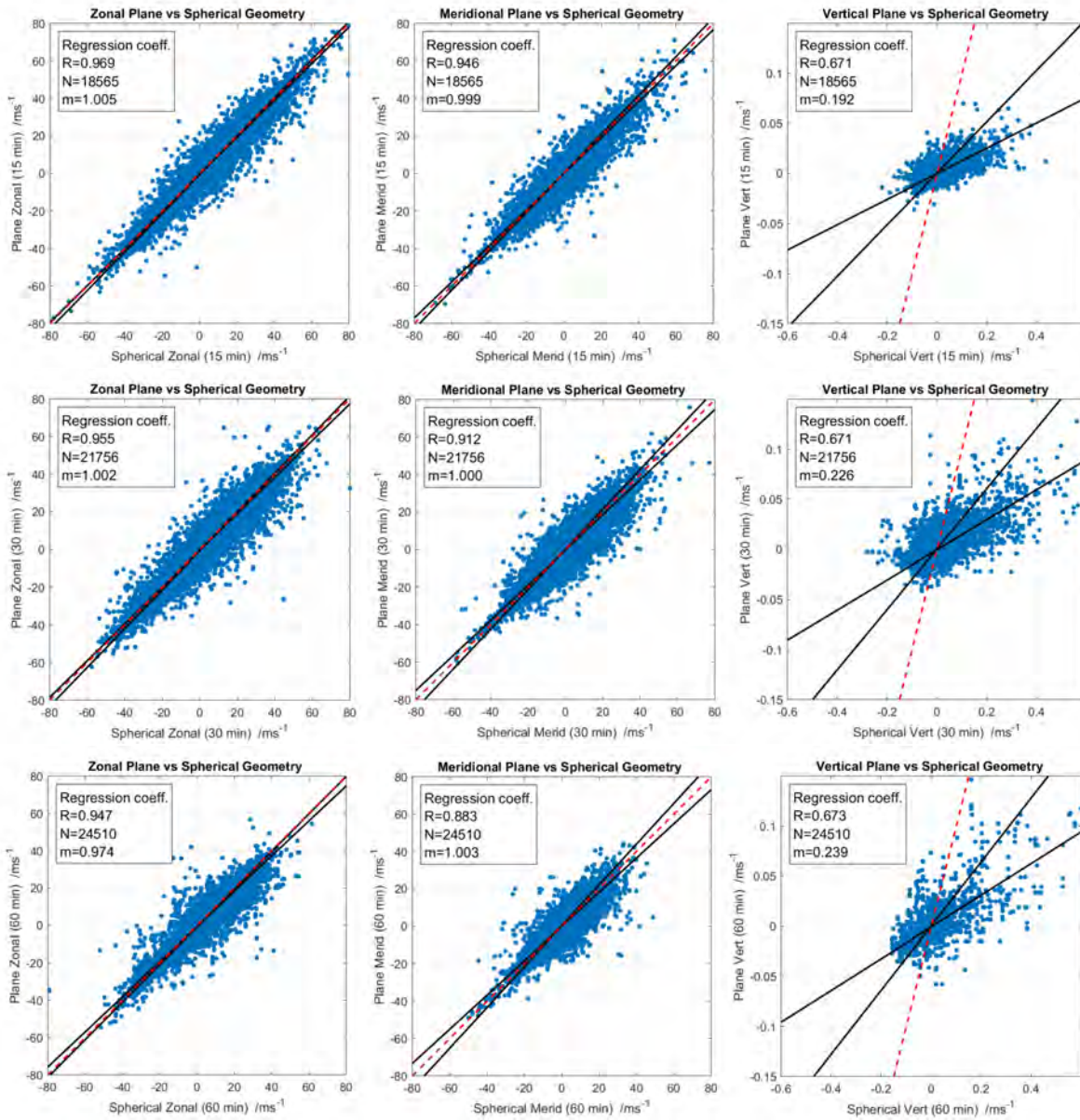


Figure S32. Same as Figure S29, but for a 350 km averaging radius and a temporal resolution of 15 (first panel), 30 (second panel), and 60 (third panel) minutes.

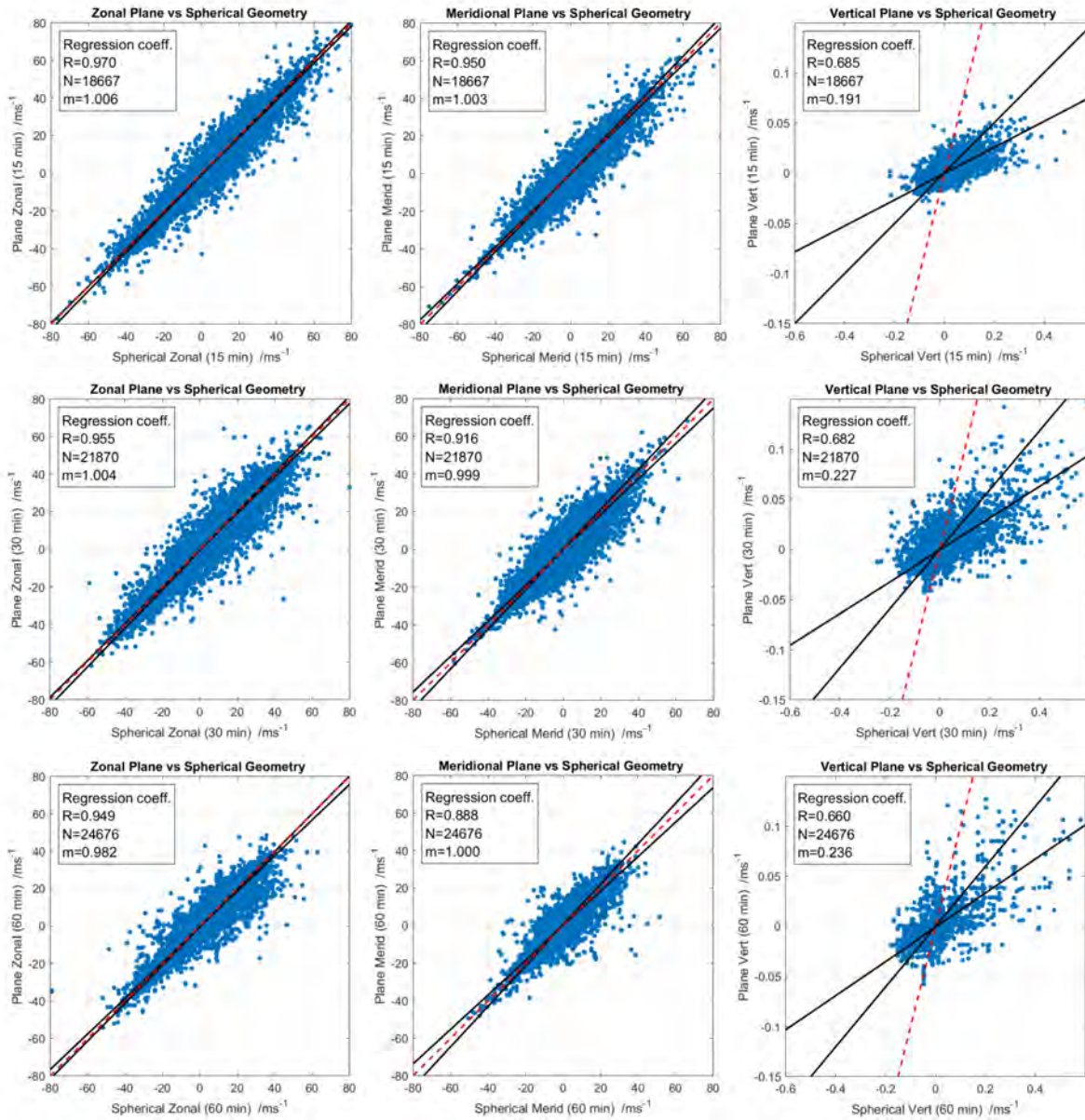


Figure S33. Same as Figure S29, but for a 400 km averaging radius and a temporal resolution of 15 (first panel), 30 (second panel), and 60 (third panel) minutes.

Correlation intercomparison of daily mean zonal, meridional, and vertical wind components computed using three temporal resolutions (15, 30, and 60 minutes) under spherical geometry for averaging radii of 200, 300, 350, and 400 km to evaluate the consistency of the simulated wind flow fields across varying temporal resolutions.

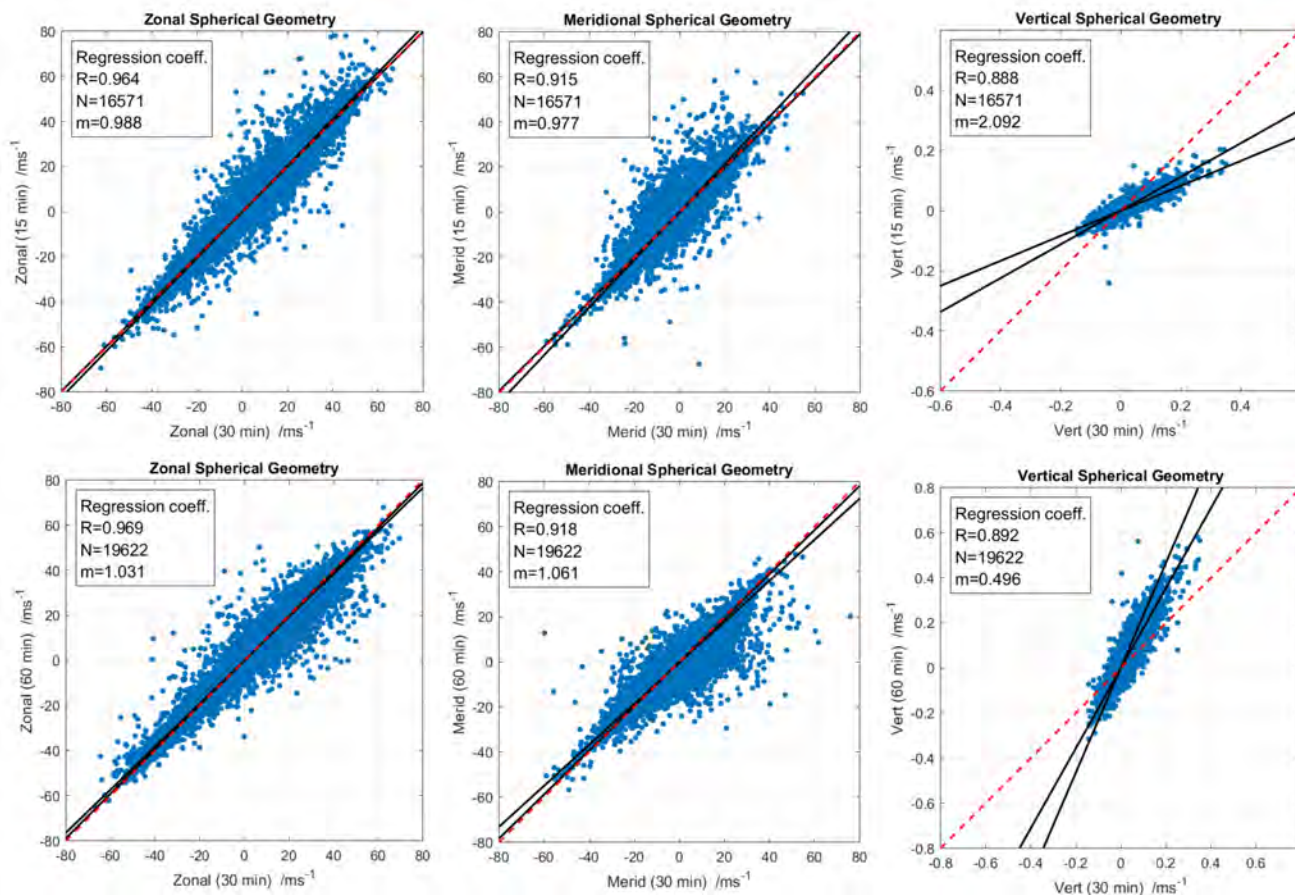


Figure S34. Correlation comparing daily mean wind velocity components (zonal, meridional, and vertical) calculated for different temporal resolutions under spherical geometry for a 200 km averaging radius. The top row compares 15-minute and 30-minute temporal resolutions, while the bottom row compares 60-minute and 30-minute temporal resolutions. Each panel shows the daily mean scatter point, robust regression fit (black solid line), 1:1 reference line (red dashed), and statistics indicating correlation coefficient (R), number of samples (N), and regression slope (m).

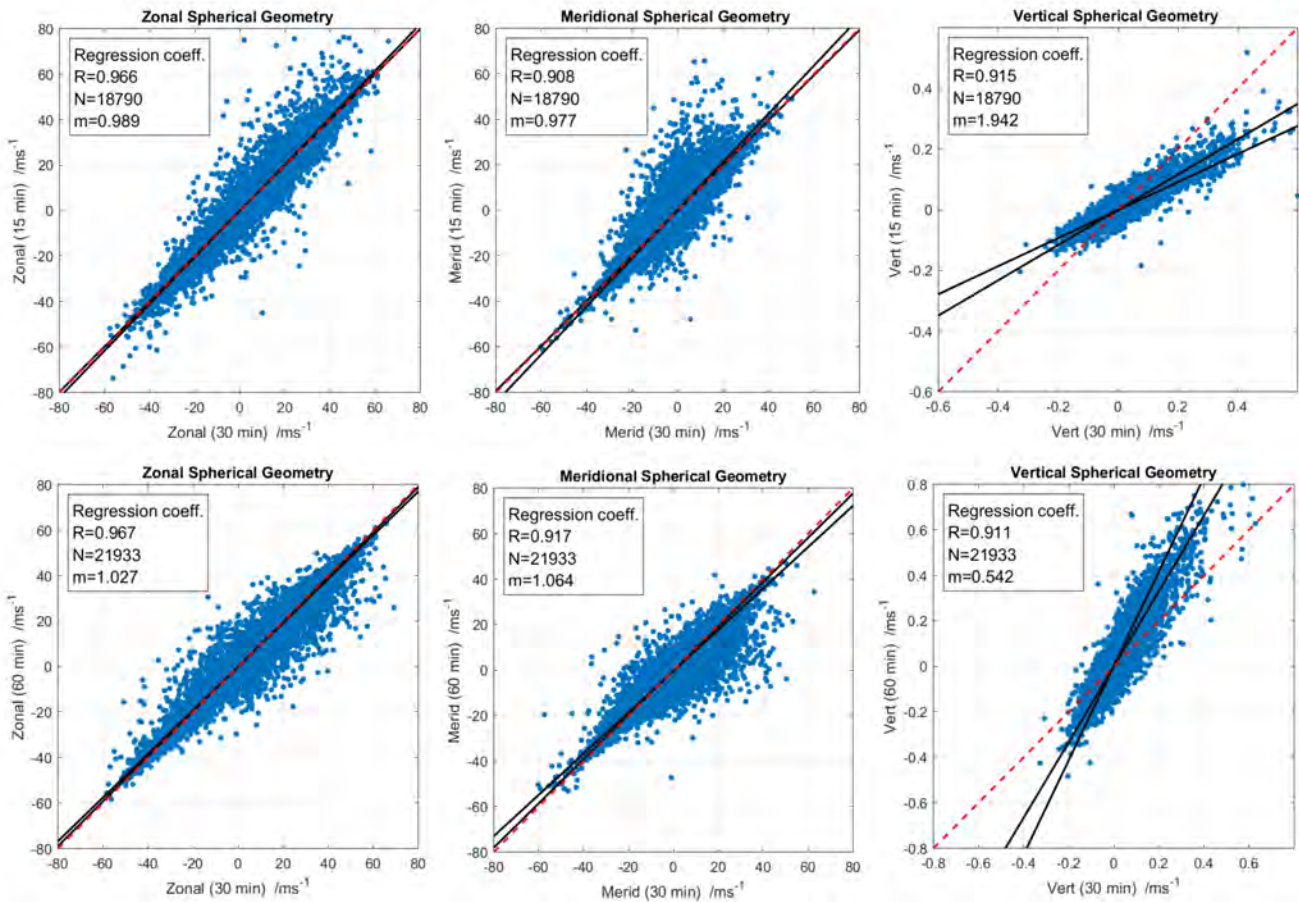


Figure S35. Same as Figure S35, but for a 300 km averaging radius and comparison between the temporal resolution of 15 (first panel) and 60 (second panel) minutes with the 30 minutes resolution.

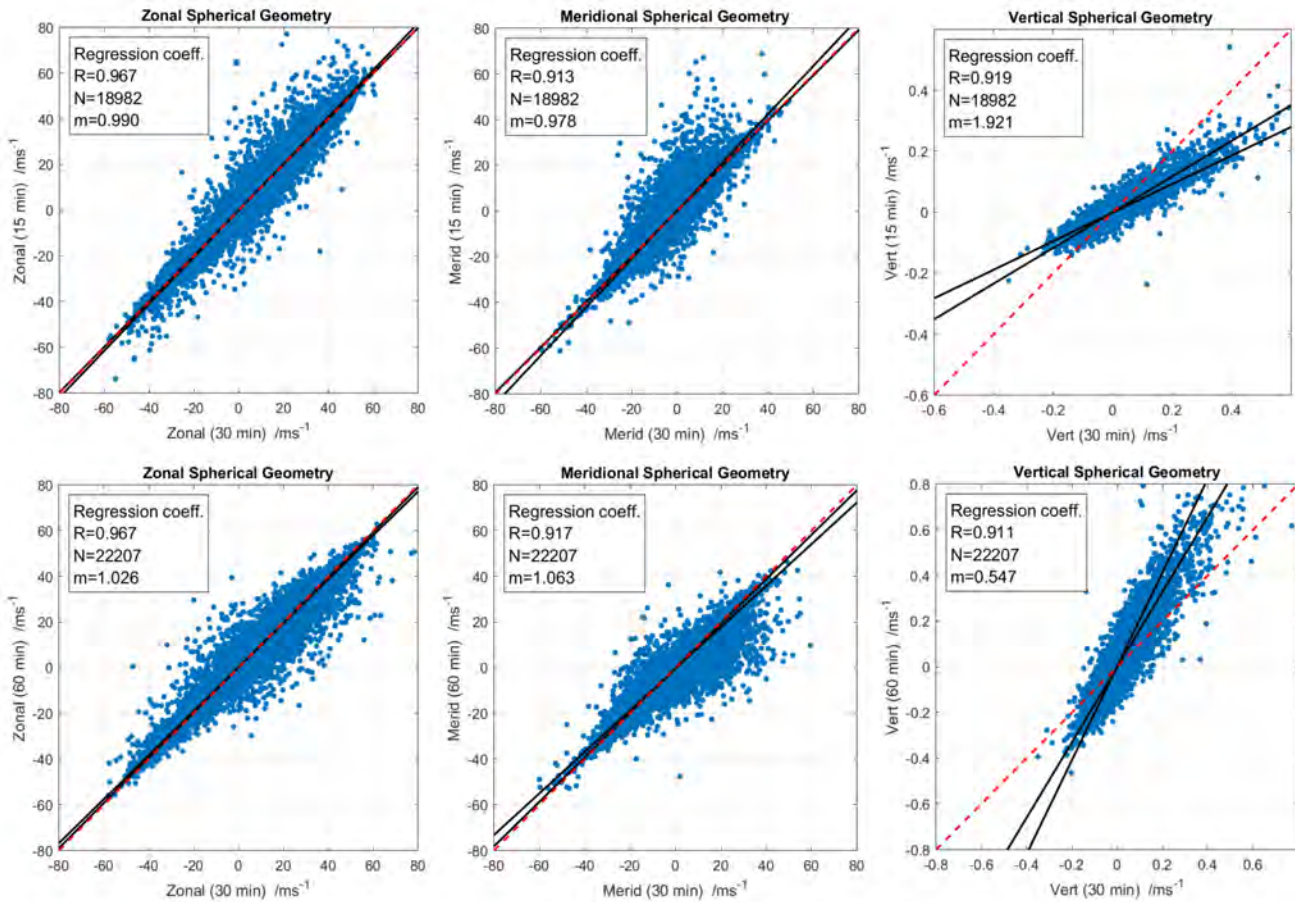


Figure S36. Same as Figure S35, but for a 350 km averaging radius and comparison between the temporal resolution of 15 (first panel) and 60 (second panel) minutes with the 30 minutes resolution.

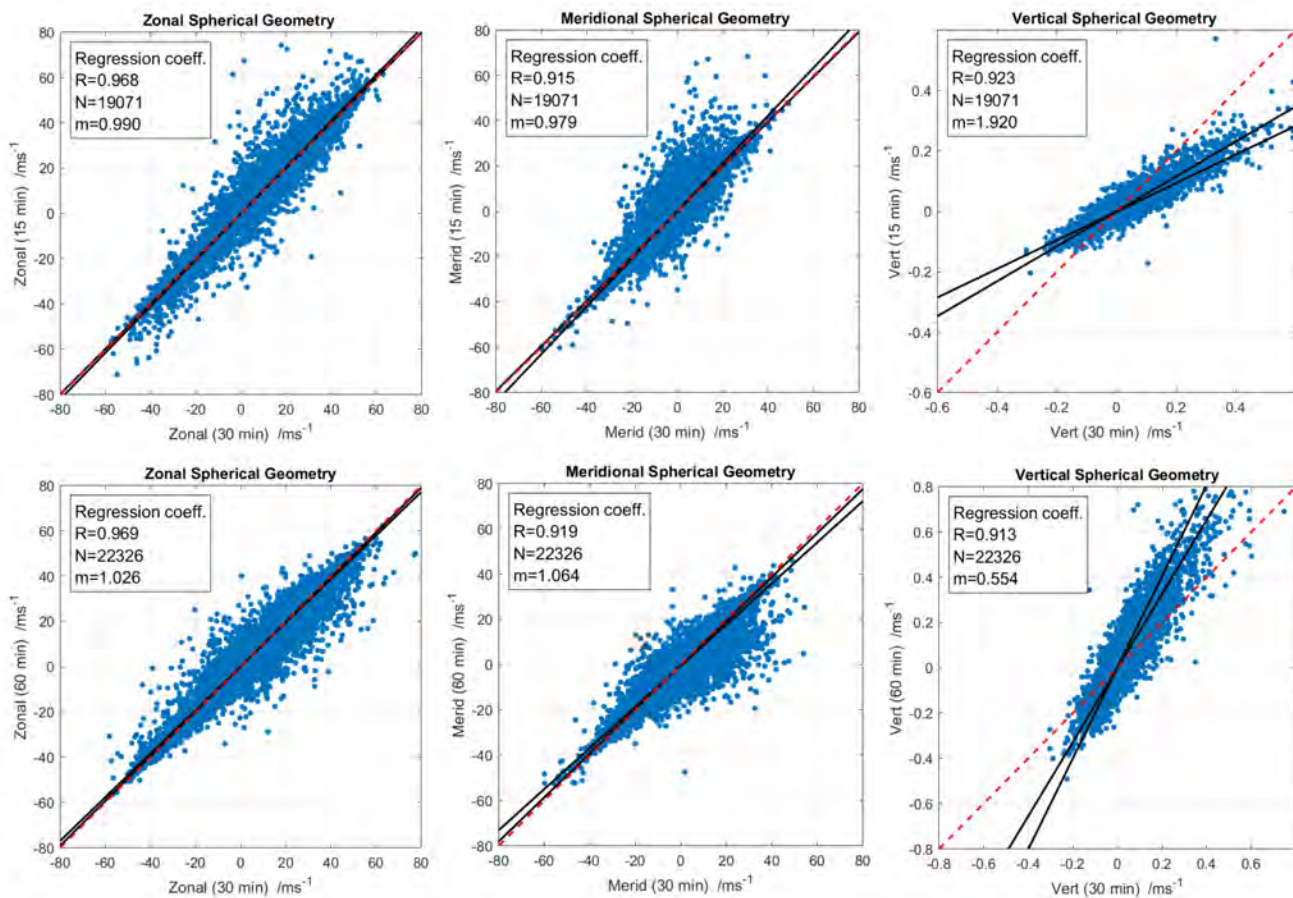


Figure S37. Same as Figure S35, but for a 400 km averaging radius and comparison between the temporal resolution of 15 (first panel) and 60 (second panel) minutes with the 30 minutes resolution.

Correlation intercomparison of daily mean zonal, meridional, and vertical wind components computed using three temporal resolutions (15, 30, and 60 minutes) under plane geometry for averaging radii of 200, 300, 350, and 400 km to evaluate the consistency of the simulated wind flow fields across varying temporal resolutions.

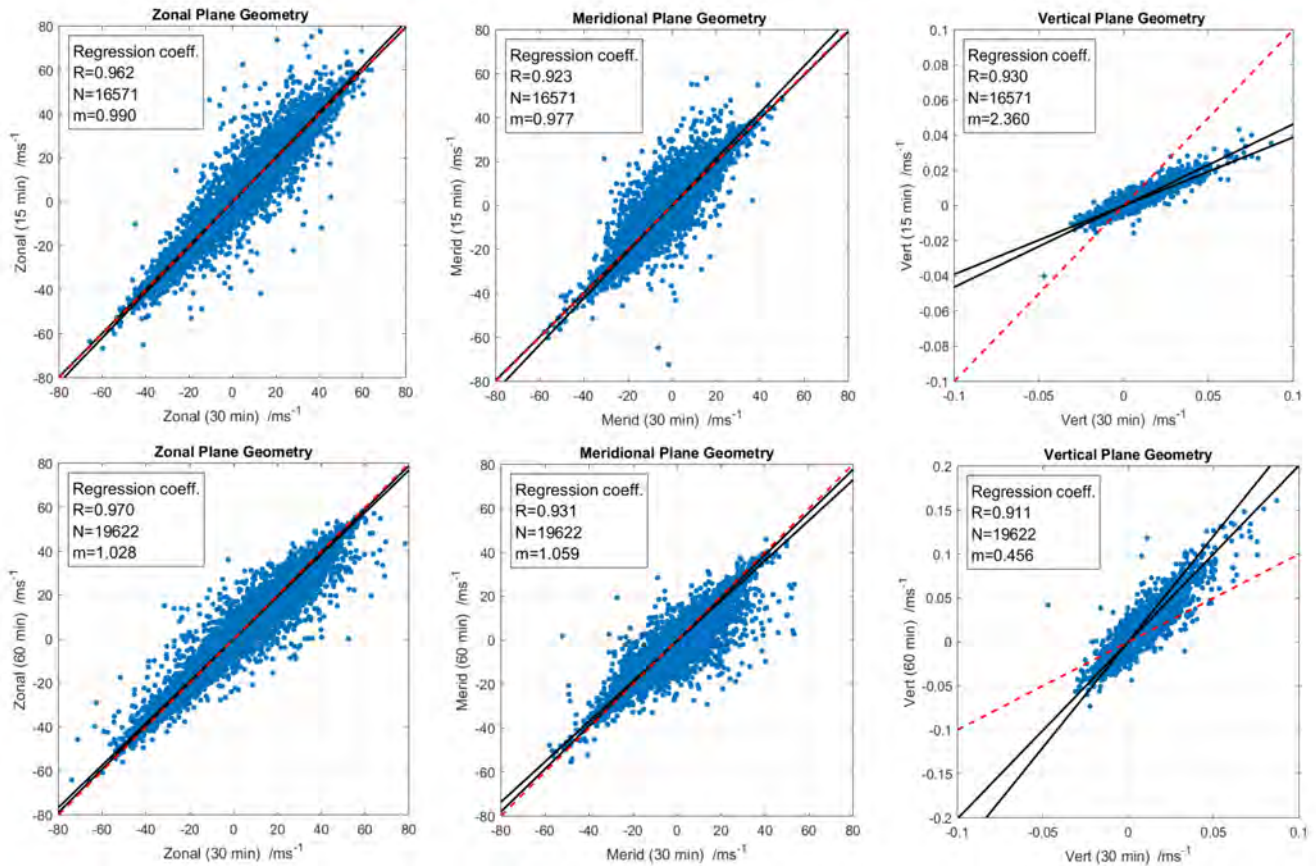


Figure S38. Correlation comparing daily mean wind velocity components (zonal, meridional, and vertical) calculated for different temporal resolutions under plane geometry for a 200 km averaging radius. The top row compares 15-minute and 30-minute temporal resolutions, while the bottom row compares 60-minute and 30-minute temporal resolutions. Each panel shows the daily mean scatter point, robust regression fit (black solid line), 1:1 reference line (red dashed), and statistics indicating correlation coefficient (R), number of samples (N), and regression slope (m).

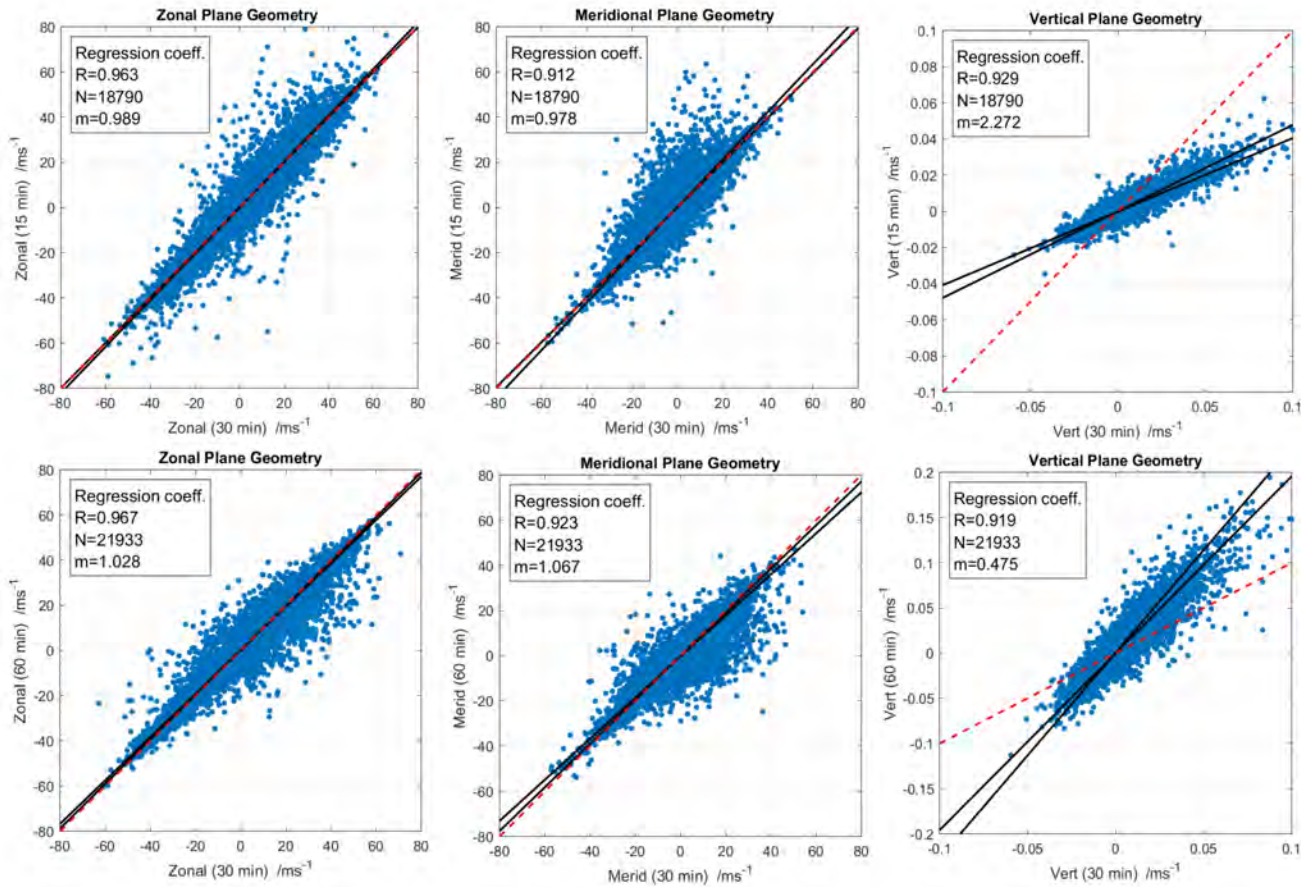


Figure S39. Same as Figure S39, but for a 300 km averaging radius and comparison between the temporal resolution of 15 (first panel) and 60 (second panel) minutes with the 30 minutes resolution.

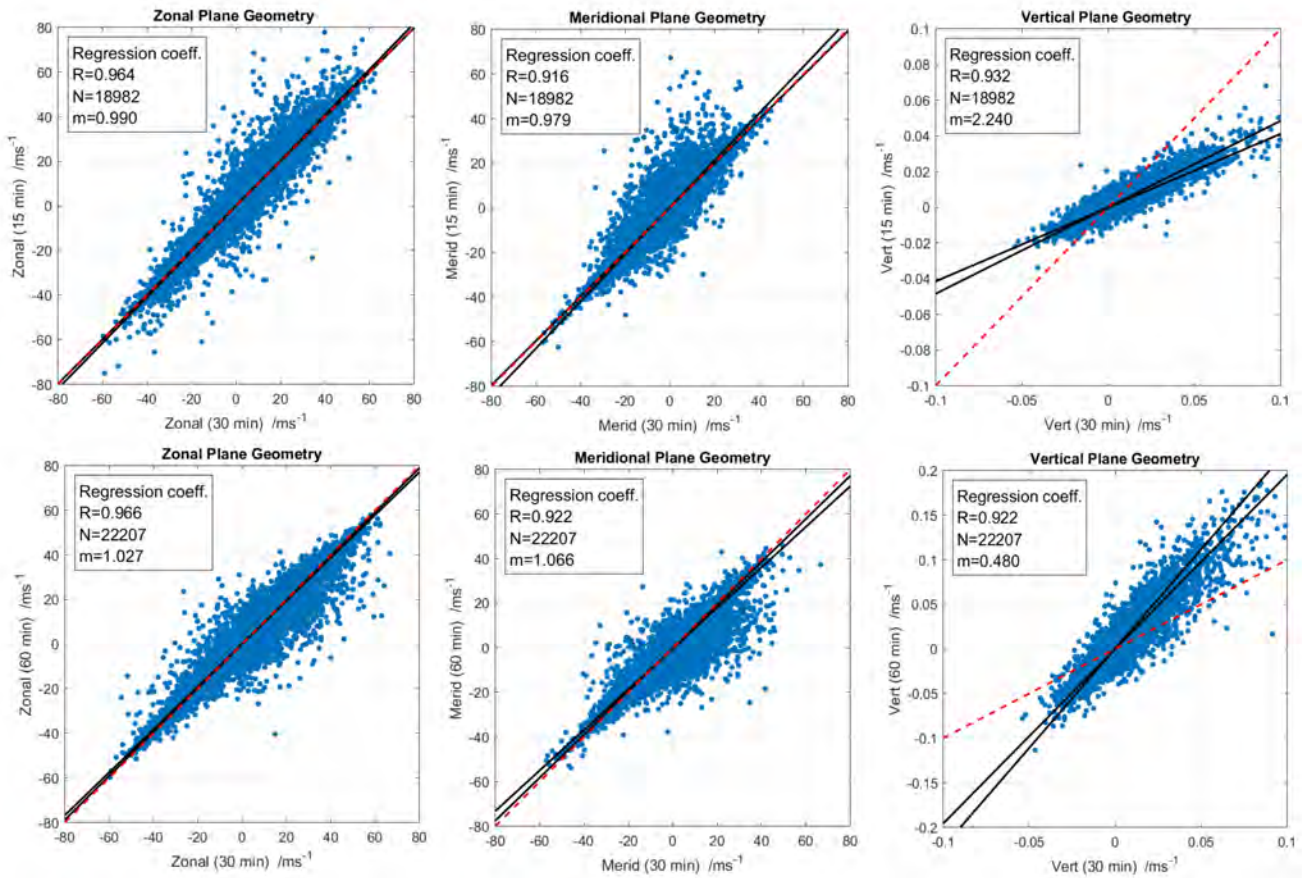


Figure S40. Same as Figure S39, but for a 350 km averaging radius and comparison between the temporal resolution of 15 (first panel) and 60 (second panel) minutes with the 30 minutes resolution.

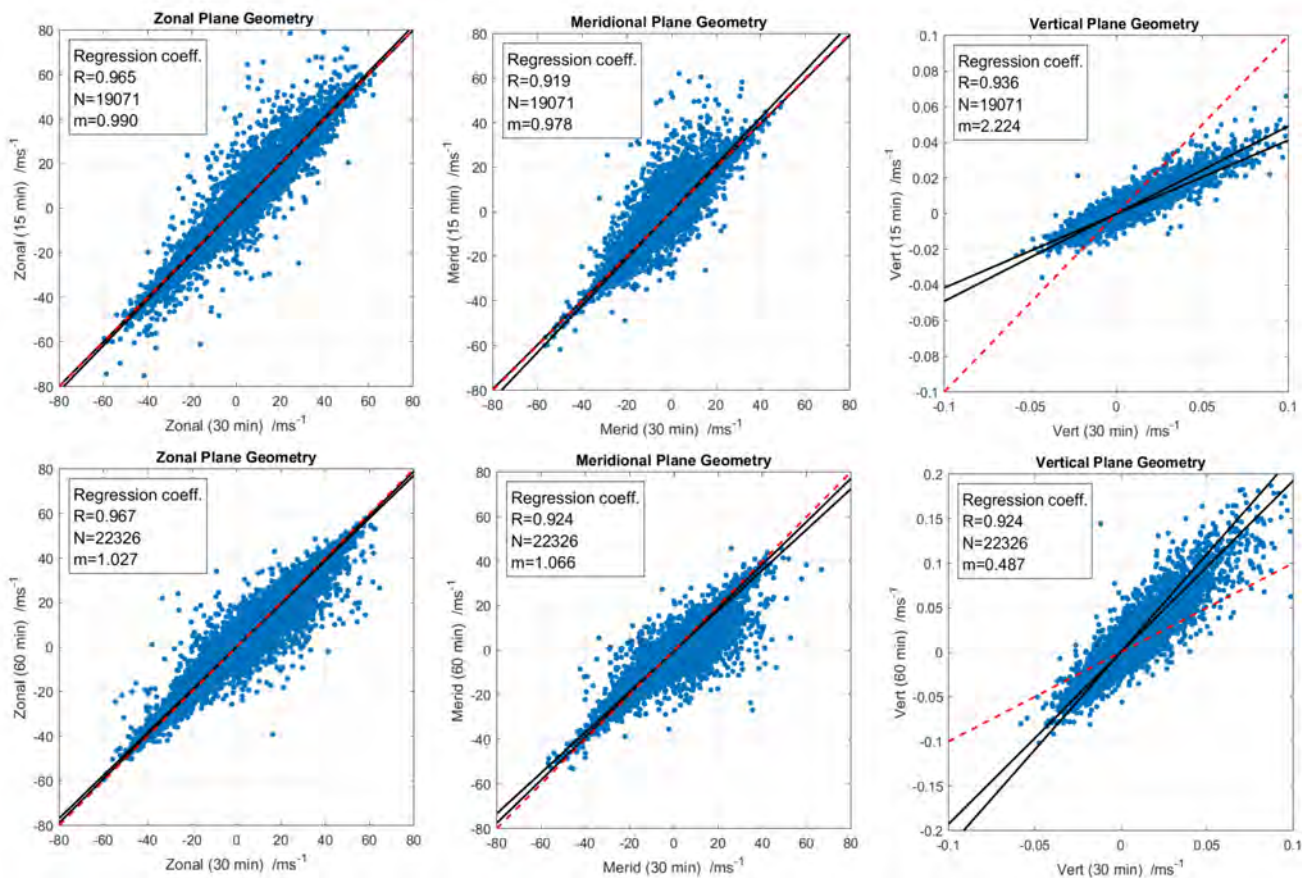


Figure S41. Same as Figure S39, but for a 400 km averaging radius and comparison between the temporal resolution of 15 (first panel) and 60 (second panel) minutes with the 30 minutes resolution.

We present an intercomparison of the higher-order kinematic variables, including horizontal divergence, shearing deformation, stretching deformation, and relative vorticity components derived under spherical geometry for three temporal resolutions (15, 30, and 60 minutes).

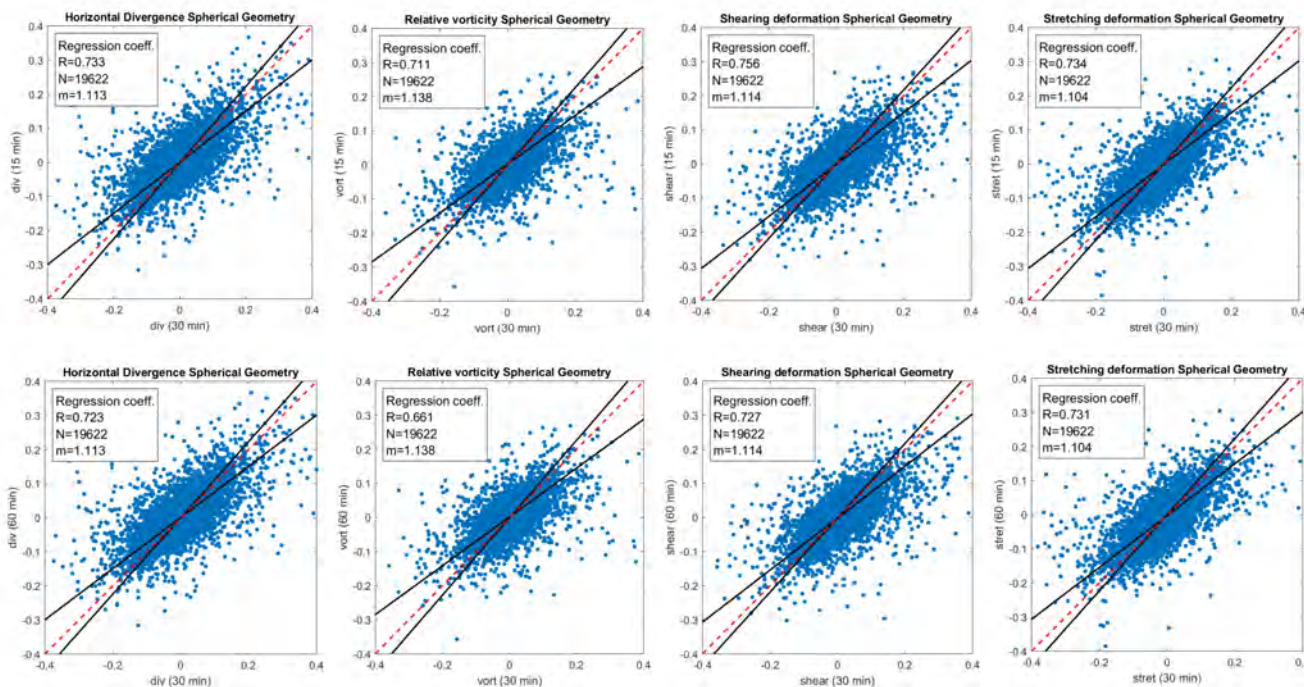


Figure S42. Comparison correlation of high-order kinematic variables; horizontal divergence, shearing deformation, stretching deformation, and relative vorticity computed for different temporal resolutions under spherical geometry for a 200 km averaging radius. The top row compares 15-minute and 30-minute temporal resolutions, while the bottom row compares 60-minute and 30-minute temporal resolutions. Each panel presents daily mean scatter points, robust regression fits (black solid line), 1:1 reference lines (red dashed), and statistics indicating correlation coefficient (R), number of samples (N), and regression slope (m).

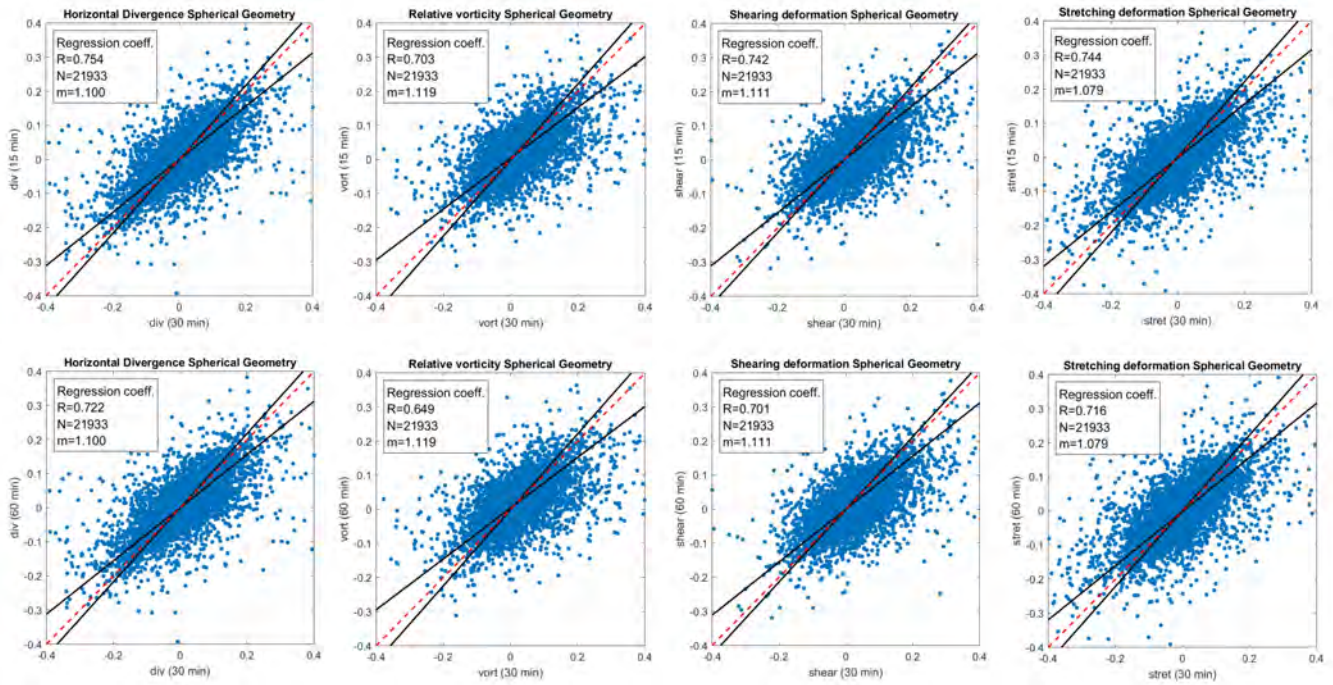


Figure S43. Same as Figure S42, but for a 300 km averaging radius and comparison between the temporal resolution of 15 (first panel) and 60 (second panel) minutes with the 30 minutes resolution.

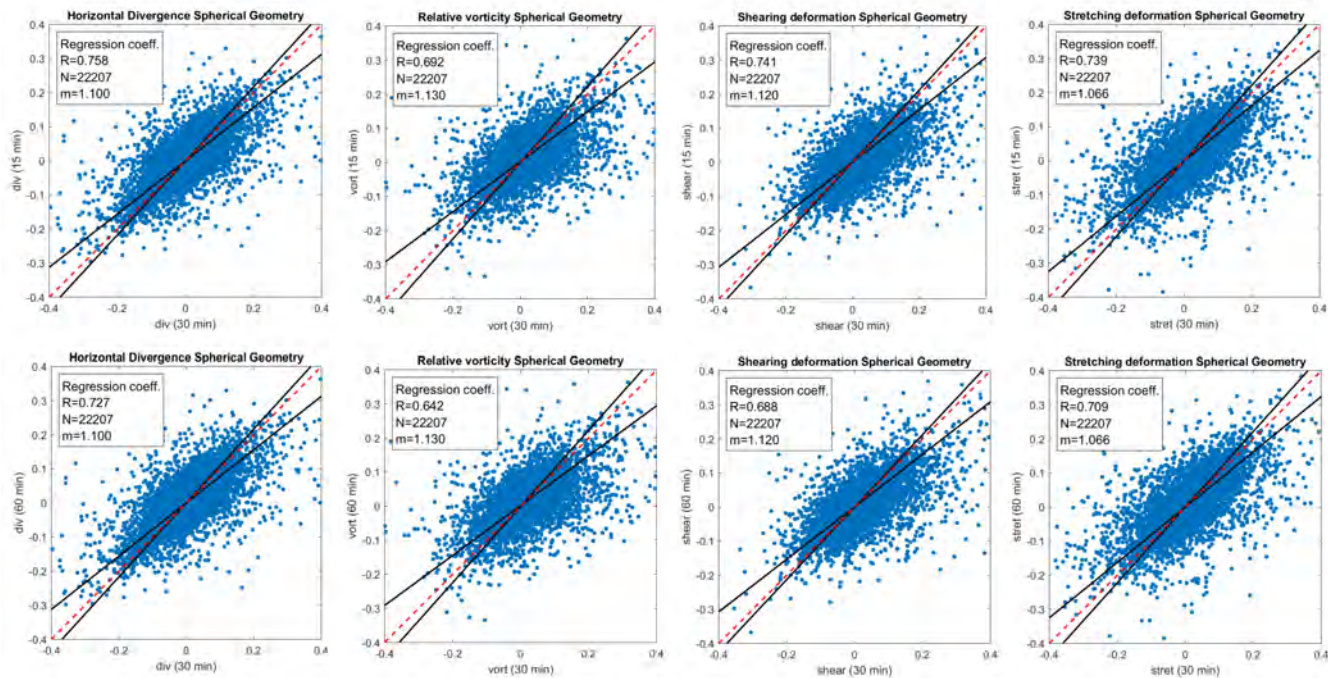


Figure S44. Same as Figure S42, but for a 350 km averaging radius and comparison between the temporal resolution of 15 (first panel) and 60 (second panel) minutes with the 30 minutes resolution.

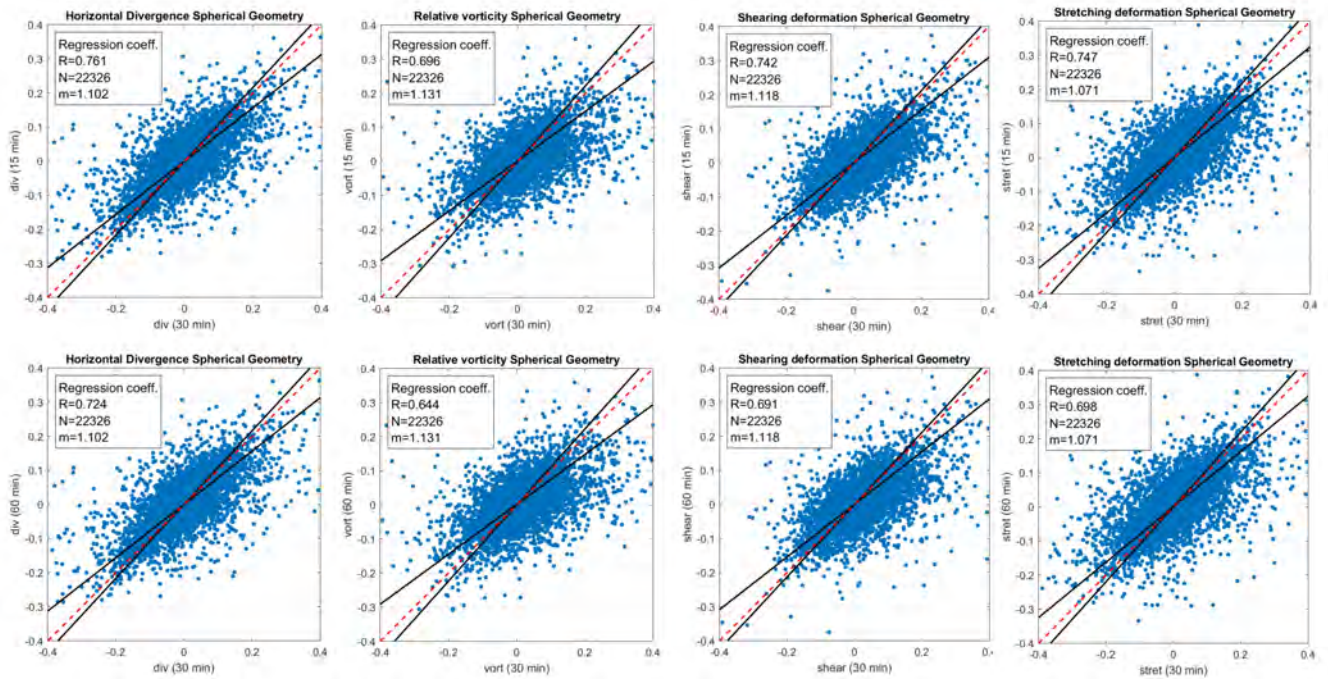


Figure S45. Same as Figure S42, but for a 400 km averaging radius and comparison between the temporal resolution of 15 (first panel) and 60 (second panel) minutes with the 30 minutes resolution.

25 We present an intercomparison of the higher-order kinematic variables, including horizontal divergence, shearing deformation, stretching deformation, and relative vorticity components derived under plane geometry for three temporal resolutions (15, 30, and 60 minutes).

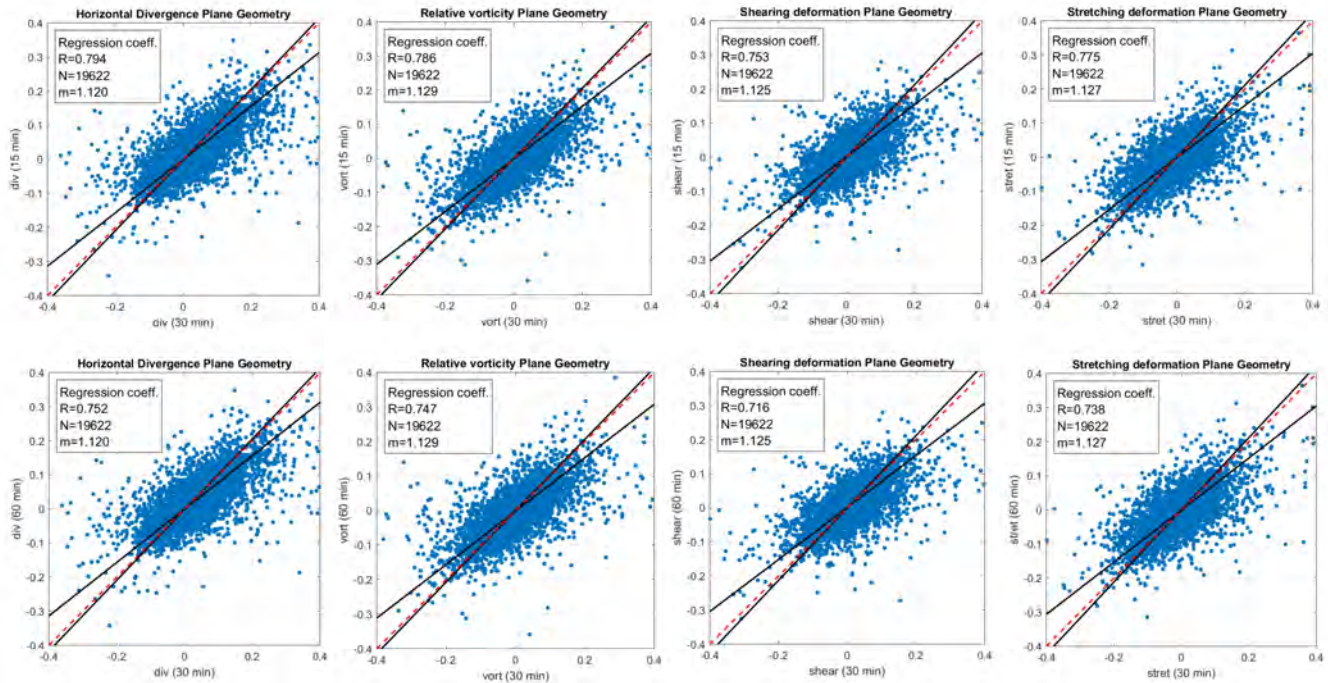


Figure S46. Comparison correlation of high-order kinematic variables; horizontal divergence, shearing deformation, stretching deformation, and relative vorticity computed for different temporal resolutions under plane geometry for a 200 km averaging radius. The top row compares 15-minute and 30-minute temporal resolutions, while the bottom row compares 60-minute and 30-minute temporal resolutions. Each panel presents daily mean scatter points, robust regression fits (black solid line), 1:1 reference lines (red dashed), and statistics indicating correlation coefficient (R), number of samples (N), and regression slope (m).

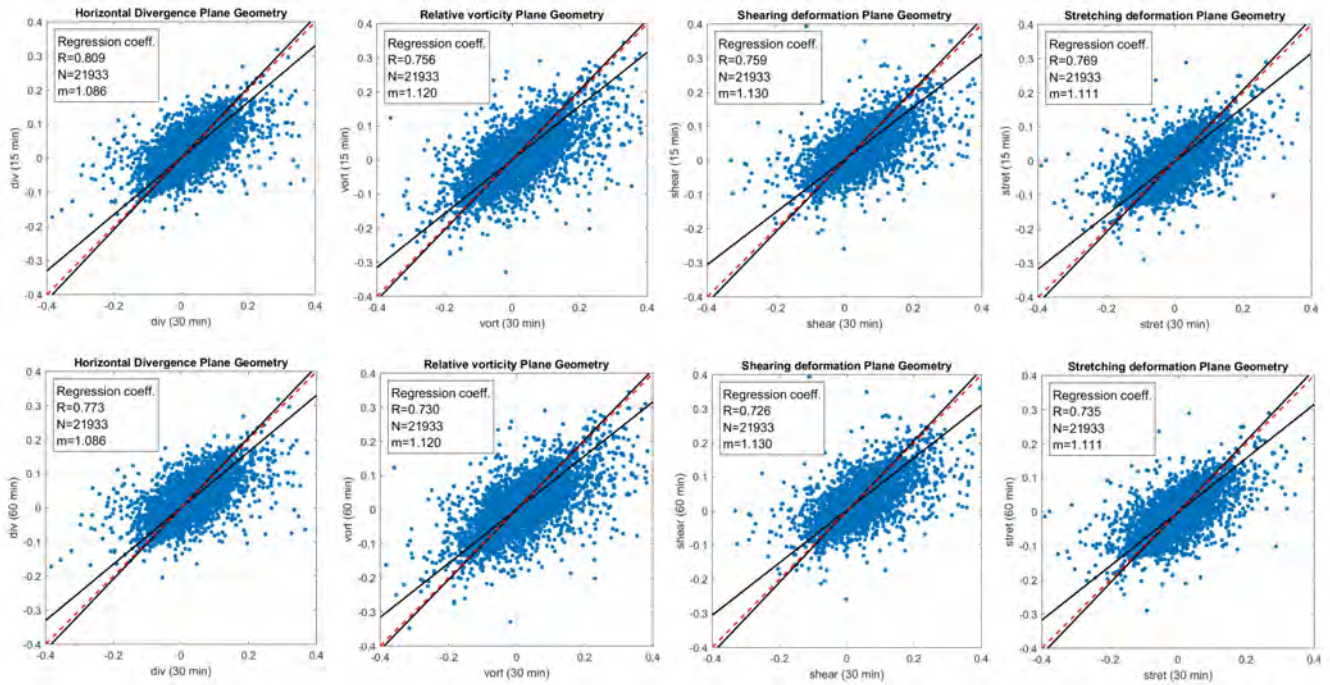


Figure S47. Same as Figure S46, but for a 300 km averaging radius and comparison between the temporal resolution of 15 (first panel) and 60 (second panel) minutes with the 30 minutes resolution.

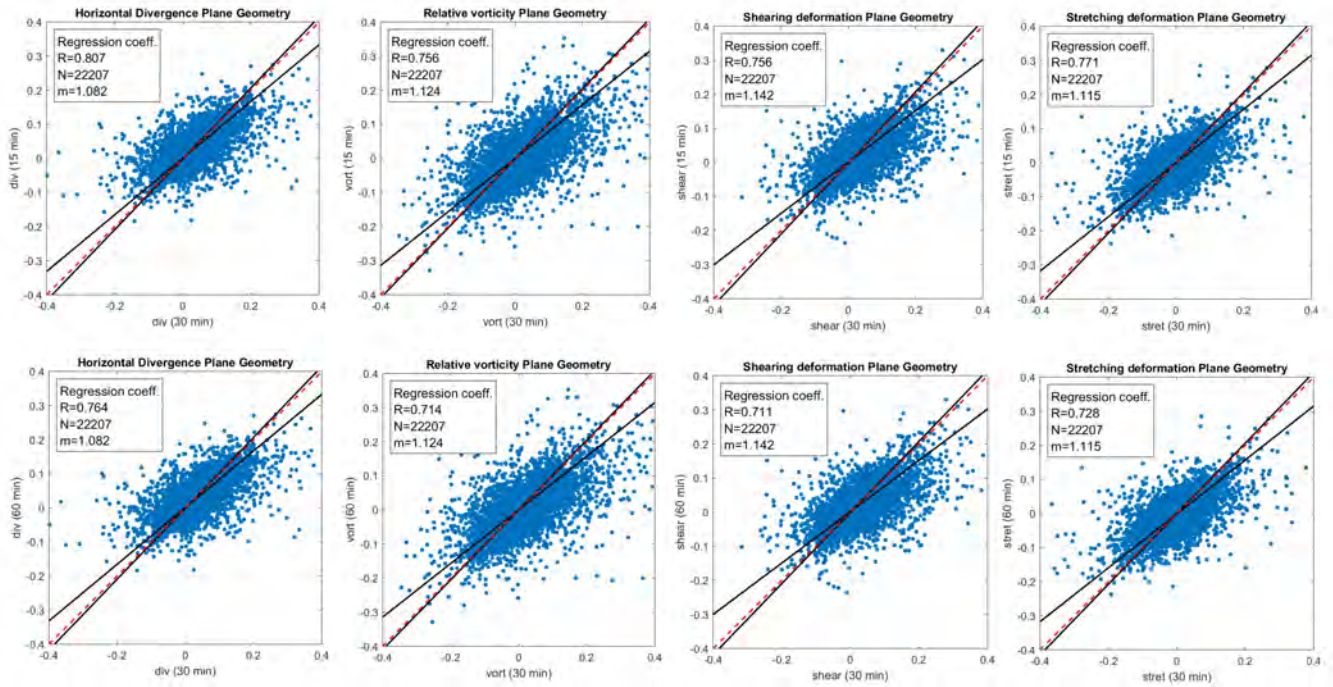


Figure S48. Same as Figure S46, but for a 350 km averaging radius and comparison between the temporal resolution of 15 (first panel) and 60 (second panel) minutes with the 30 minutes resolution.

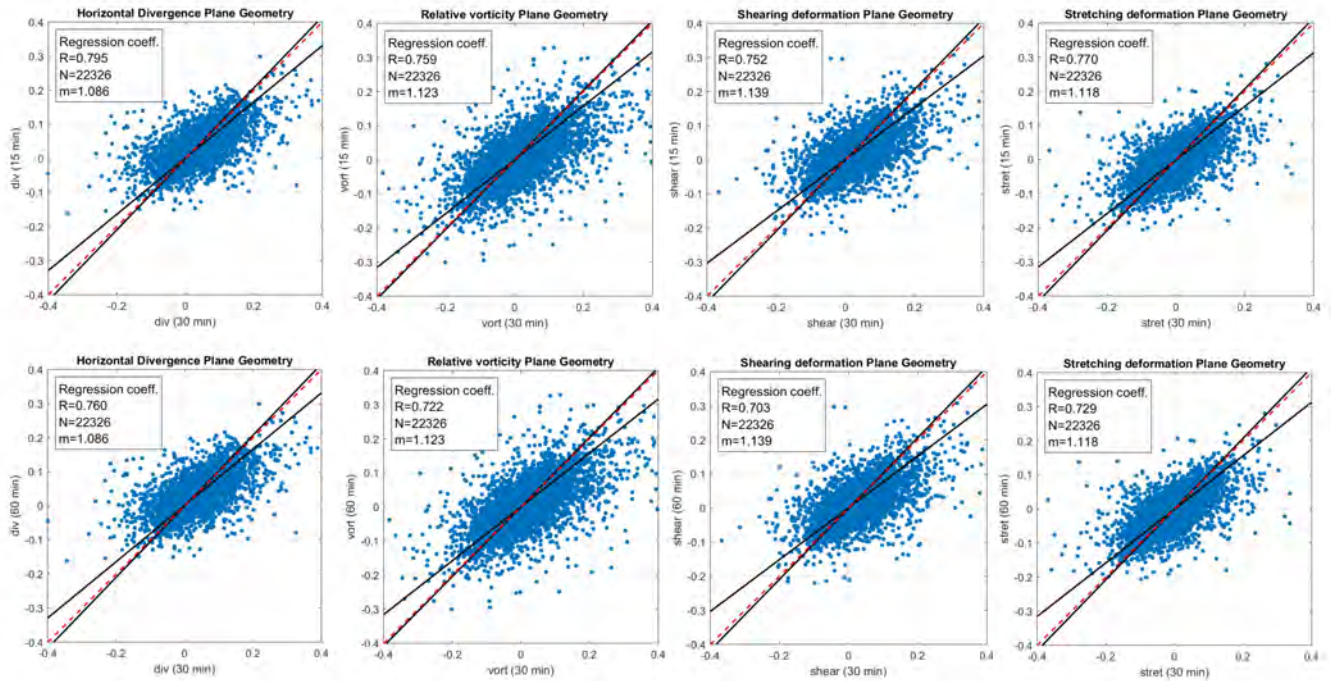


Figure S49. Same as Figure S46, but for a 400 km averaging radius and comparison between the temporal resolution of 15 (first panel) and 60 (second panel) minutes with the 30 minutes resolution.